Improving the performance of the SLIMR design

Introducing a 3-pass core design and neutronic-thermalhydraulic coupling

Dennis Krijger

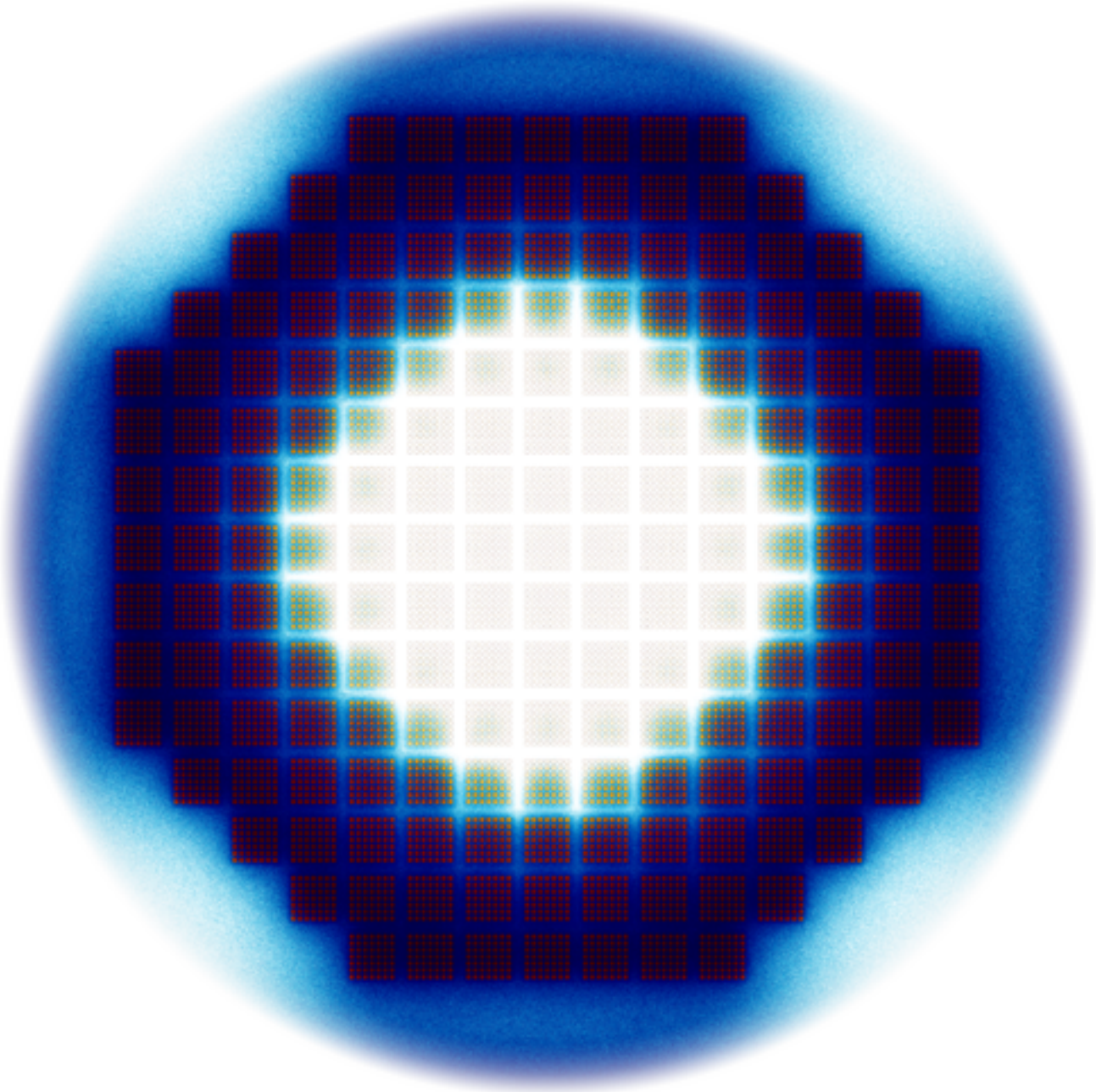

TU Delft

IMPROVING THE PERFORMANCE OF THE S L I M R DESIGN

INTRODUCING A 3-PASS CORE DESIGN AND NEUTRONIC-THERMALHYDRAULIC COUPLING

by

Dennis Krijger

in partial fulfillment of the requirements for the degree of

Master of Science

in Sustainable Energy Technology

at the Delft University of Technology,

to be defended publicly on Friday November 13, 2015 at 01:00 PM.

Student number:	4081522	
Supervisors:	Prof. dr. ir. J.L. Kloosterman,	
	Dr. ir. M. Rohde	
Thesis committee:	Prof. dr. ir. J.L. Kloosterman,	TU Delft
	Prof. dr. ir. B.J. Boersma,	TU Delft
	Dr. ir. M. Rohde	TU Delft

Nomenclature

Latin symbols

Symbol	Units	Description
A	m^2	Area
c_p	$Jkg^{-1}K^{-1}$	Specific heat
C	m^{-3}	Precursors density
d	m	Distance between nodes
D	m^{-1}	Diffusion coefficient
D_H	m	Hydraulic diameter
E	J	Energy
G	$kgm^{-2}s^{-2}$	Mass flux
h	$Wm^{-2}K^{-1}$	Heat transfer coefficient
k	—	Multiplication factor
l	s	Neutron life time
L	m	Length
M	kgs^{-1}	Mass flow rate
n	m^{-3}	Neutron density
$\mathbf{n}$	—	Unit normal vector
N	—	Total number of neighbouring nodes
P	W	Power
P_w	m	Wetted perimeter
p	Pa	Pressure
q''	$Jm^{-2}s^{-1}$	Surface heating rate
q'''	$Jm^{-3}s^{-1}$	Volumetric heating rate
t	s	Time
T	°C	Temperature
v	ms^{-1}	Speed
V	m^3	Volume
w	J	Energy released during a fission event

Greek symbols

Symbol	Units	Description
α_{ii} or α_{ij}	—	Coupling coefficients
α	K^{-1}	Reactivity feedback coefficients

β	$-$	Fraction of a delayed fission neutron group
η	$-$	Thermal efficiency
λ	s^{-1}	Decay constant
λ	$Wm^{-1}K^{-1}$	Thermal conductivity
Λ	s	Generation time
ν	$-$	Neutron yield
ρ	$-$	Reactivity
ρ_m	kgm^{-3}	Moderator density
Σ	m^{-1}	Macroscopic cross-section
ϕ	$m^{-2}s^{-1}$	Neutron flux

Subscripts

a	absorption
f	fission
f	fuel
i	i^{th} node
j	neighbouring node
k	k^{th} delayed neutron group
m	moderator
r	relative
rod	fuel rod
SS	Steady state
cyl	cylinder jacket

Superscripts

n	time step
$'$	deviation from steady state

Dimensionless numbers

N_{pch}	Pseudo phase change number
N_{sub}	Subcooling number
Nu	Nusselt number
Pr	Prandtl number
Re	Reynolds number

Acronyms

AECL	Atomic Energy of Canada Limited
BOC	Beginning of life cycle
B&W	Babcock & Wilcox
BWR	Boiling Water Reactor
CHF	Critical Heat Flux
CHRS	Containment Heat Removal System
DHRS	Decay Heat Removal System
DOE	Department of Energy
EOC	End of life cycle
ESBWR	Economic Simplified Boiling Water Reactor
FVM	Finite Volume Method
FA	Fuel Assembly
GIF	Generation IV International Forum
HPLWR	High Performance Light Water Reactor
HTD	Heat Transfer Deterioration
HTR-PM	High-Temperature Reactor Pebble bed Module
iPWR	integral Pressurized Water Reactor
LOCA	Loss of Coolant Accident
LR	Large Reactor
LWR	Light Water Reactor
MCNP	Monte Carlo N-Particle
MHTGR	Modular High-Temperature Gas-cooled nuclear Reactor
NSSS	Nuclear Steam Supply System
RPV	Reactor Pressure Vessel
SCRAM	Safety Control Rod Axe Man
SLIMR	Small-scale, Large efficiency, Inherently safe, Modular Reactor
SMR	Small to Medium-sized Reactors or Small Modular Reactor
SSR	Super-Safe Reactor
STAFAS	Sub-channel Thermal-hydraulics Analysis of a Fuel Assembly under Supercritical conditions
WSMR	Westinghouse Small Modular Reactor

Abstract

Small Modular Reactors (SMRs) are gaining more attention in the field of nuclear engineering. Their potential for passive decay heat removal increases safety and their modularity enlarges the employment variety and creates investment opportunities. Rohde [27] proposed a concept design for a SMR: the SLIMR (a Small-scale, Large efficiency, Inherently safe, Modular Reactor). Veling [36] performed a thermal hydraulic feasibility study in terms of safety of the SLIMR design. The first design of the SLIMR showed potential with respect to safety, but improvements in thermal power and the efficiency of the reactor were necessary. Furthermore, only the thermal hydraulic stability of the natural circulated flow of the supercritical water in the SLIMR was studied. The feedback mechanisms between the neutronics and the thermal hydraulics were not modeled in the work of Veling [36].

This research made progress towards improving the design of the SLIMR with respect to its performance (i.e. power and efficiency) and including coupling of the neutronics and thermal hydraulics in the SLIMR model [36]. The main research question that is answered is:

"*How can the SLIMR design be made feasible, while meeting performance and stability standards?*"

To answer this question, three sub-questions are answered first:

1. What are optimal design parameters to increase the performance of the SLIMR including the three-pass core configuration?
2. How can the small reactor core be made critical under supercritical conditions?
3. How does the coupling of the thermal hydraulics and the neutronics have an effect on the stability of the SLIMR?

The one-pass core design of the SLIMR is substituted by a three-pass core design (based on the HPLWR core design) and with the numerical SLIMR model a parameter study is performed. Subsequently this new core design is evaluated on its neutronic characteristics with the use of a three-dimensional continuous-energy Monte Carlo reactor physics burn-up calculation code, named *Serpent* [18]. Afterwards, with the calculated reactivity feedback coefficients and the coupling between the neutronics and thermal hydraulics a stability analysis is performed.

It was found that with the three-pass core design the SLIMR is able to ensure a stable system which reaches 350 MWth with a core outlet temperature of 396 °C, when a riser with a length of 9 m is placed on top of the core. The reactivity feedback coefficients were found to be positive for the moderator density feedback and negative for the Doppler feedback, which leads to a negative feedback. No instabilities were found for the following range of the operational parameters, i.e. the power was varied from 100 MW to 440 MW and the inlet temperature was varied from 250 °C to 350 °C. Though, it has been shown that the heat transfer coefficient of the fuel pin's surface to the coolant could have significance influence on the

response of the system to perturbations. When heat transfer deterioration occurs the small heat transfer coefficient introduces a delay between the heat transfer and the generated power in the system, which results in perturbations remaining longer in the system because of the delayed feedback, i.e. a less stable system.

Acknowledgements

I hereby want to express my gratitude towards my supervisors, Jan Leen Kloosterman and Martin Rohde, who offered me a great project and helped me along the way. They steered me in the right direction and gave constructive feedback on my work. Also I want to thank the NERA department for the company during the project. I had a great time doing my bachelor thesis two years ago and it made me wanted to come back for my master thesis.

D. Krijger
Delft, November 2015

Contents

Chapter 1

Introduction

In the search for more sustainable, reliable, and foremost safe nuclear reactors Small Modular Reactors (SMRs) are gaining more attention. Accidents in the past with nuclear reactors have shown us that safety is and should be priority number one during the design of a nuclear reactor. However, for one to take upon the endeavour to build and operate a reactor for the generation of power, it should also be attractive from an environmental and economical point of view. So besides improving safety other practices are important as well, such as increasing the efficiency, decreasing production of radioactive waste and solving proliferation issues. Because SMRs are smaller than their bigger brothers, they benefit from certain advantages. For example, SMRs can provide a wide range of power due to their modular nature. Multiple modules can be placed at one power plant facility to meet the required power demand. Also from an economical point of view SMRs could be standardized and enjoy economies of scope rather than economies of scale. This is in contrast with large-scale nuclear reactors, which often require a more specialized design and have to fit the surroundings and meet stricter requirements. Furthermore, due to its smaller size passive decay heat removal processes are possible during emergency scenarios, thus increasing the overall safety of the reactor. So in short, there are enough reasons to research the feasibility of various SMR designs.

In this context of SMRs Rohde [27] of the department NERA of the Reactor Institute Delft has proposed a preliminary design for a SMR; the SLIMR (a Small-scale, Large efficiency, Inherently safe, Modular Reactor). Veling [36] has done a parameter study into the feasibility of this reactor design with respect to its safety. This research continues with his work, but before presenting the aim of this research a more elaborate introduction is given to the concept of SMRs, the SLIMR design is described and an overview of previous research is presented.

1.1 Small Modular Reactors

1.1.1 The advantages and challenges of SMRs

Throughout literature the abbreviation SMR is used in two ways, either it is used to indicate Small-to-Medium sized Reactors, or it refers to Small Modular Reactors. When the latter one is meant, focus lies usually at the ”modular” part. A power plant can for example consist out of multiple SMRs, which contribute to an overall desired power level. Also, modular could refer to coupling of the Nuclear Steam Supply System (NSSS) with a process heat supply system or power conversion system. Small, in both

meanings, refers to the expected power output of the reactor, ranging between 10 and 300 MWe. Medium sized reactors go up to 700 MWe [34]. However, with both abbreviations the same concept of reactor is usually meant. In the next two sections the advantages and disadvantages that come along with SMRs designs are being elaborated.

Advantages

First of all, the fact that SMRs are small gives them a number of advantages compared to Large Reactors (LRs). To begin with, SMRs are suitable to small electric grids in areas where LRs are not an option. Either there is no site able to accommodate such a large nuclear power plant or the large capacity exceeds the local power demand and budget constraints. SMRs however can more easily meet local power demands [12]. Also, due to their smaller size SMRs can be manufactured off site and be transported as a whole to the specific location. Components for LRs can also be manufactured off site and be transported as well, but in many cases a lot of work on site is necessary. Especially for remote areas this work on site can become costly when workers and materials have to travel long distances. SMRs can be designed in such way that the whole system can be transported at once, either by heavy-duty trucks, rail or by barge [20]. On site construction is then reduced as the system is to be transported completely to the specific site. Furthermore, a smaller nuclear core enables passive heat removal processes during emergencies. The amount of decay heat is smaller and the area-to-volume ratio is beneficial for passive heat transfer processes. Passive heat removal ensures that intervention of operators is not necessary, which is safer during severe accidents. [29]

Secondly, the modularity of the SMRs provides advantages as well. For one, SMRs can be used not only for the production of electricity, but also for the production of heat and the process of desalination of salt water [21]. These processes can even be combined. LRs can be used for the same purpose, but their significant power capacity exceeds the power demands for these processes in many cases. The lower power capacity of SMRs is more suitable to chemical companies and steel companies. And, especially in a future where water becomes more scarce as earth's population is growing and climates are changing, desalination of water in remote areas becomes more important. Furthermore, SMRs can meet a broad range of power demands. One power module might produce up to 100 MWe, placing ten modules next to each other at one site increases the power capacity to 1000 MWe. This flexibility in power range can create a larger demand and thereby attract more investors for the development of the design. Also incorporating a number of modules instead of one big plant increases reliability and safety. During maintenance of one module the other modules can still be in operation. Even during construction of the later modules, the ones that are built first can already operate and generate income [35]. Regarding safety, employing several modules decreases the impact of severe accidents. If one module experiences an accident the other modules are not affected and could even still operate. The affected module would be shutdown and checked.

Thirdly, by making the reactor smaller and modular economic benefits can be attained. Within the nuclear industry the economies-of-scale paradigm has dominated the industry for a while. As the capacity increases the average investment and operating costs per unit of energy decreases. However, as the size of the nuclear plant increases so does the complexity and the uniqueness of the design (as it has to comply with local constraints), therefore increasing total costs [36]. In contrast with the LRs, SMRs can be built through factory fabrication. The design of the modules can be standardized and learning curves apply as the number of produced units increases, effectively driving down costs [12]. Rather than enjoying economies of scale SMRs will enjoy economies of mass production, making them economically competitive with LRs. The new designs of SMRs have also seen some simplifications. The smaller size made it possible to lower the number of (active) components and safety systems. Costs can be decreased

as designs become more simple and straightforward. [20]

Challenges

Summing up all the advantages in the previous section might raise the question why SMRs have not been employed on a larger scale than they are at the moment. For one, as mentioned before, the "economies-of-scale" paradigm has dominated the nuclear industry for quite a while and only recently focus begins to shift towards SMRs. Furthermore, according to Locatelli et al. [20], it was more convenient to use proven technologies and it used to be more simple to use pumps and tubes to control fluids instead of some of the new techniques, i.e. natural circulation. Natural circulations requires sophisticated computer simulations, which with the technology at that time (20 to 30 years ago) was not possible. Although these challenges might not seem to be the problem anymore, SMRs still face other challenges for broader implementation.

Though the modularity ensures some economic benefits, plants under 1 GW enjoy these benefits less. Fixed costs and investments are spread over a smaller power capacity and therefore the project needs to be evaluated carefully [20]. Furthermore, nuclear projects are often accompanied with a long license process and regulatory issues. Especially when the technology is not already proven or deployed somewhere else this process can take up more time and experience more hurdles. For smaller projects this larger time window might not meet short term expectations so other energy technologies will be explored [10].

In addition the financial risk perceived by investors has to be reduced. The higher perceived risk comes mainly from three factors, as argued by Todreas [34]. First, licensing requirements from regulatory institutions in countries could affect the amount of capital and height of operating costs with regard to insurance, licensing fees, plant staffing, security requirements and decommissioning funding [34]. Secondly, the learning curve promised with SMRs might not turn out as expected and leave investors with higher costs. Lastly, unpredictable events, such as the Fukushima accident, could delay construction because design criteria and construction regulations become stricter. Also severe reactor accidents and unforeseen increases in operating and maintenance costs deter investors from pursuing SMRs.

Finally, nuclear proliferation can become an issue when SMRs are being deployed on a larger scale [7]. SMRs are small and can meet a broader range of power demand, stimulating its implementation in more areas. More actors having access to nuclear materials and the decentralized handling processes of nuclear waste that come with it increase the risks of proliferation. This issue has to be taken care of in every single case of a SMR. Rules and regulations should be coherent and followed nationwide to ensure prevention of proliferation.

1.1.2 Current state of SMRs

In this small overview of the current development and deployments of SMRs five Generation III/III+ or Generation IV designs are considered. Older nuclear power reactors designs are not taken into account, because they can not compete with the new designs based on safety and performance. According to Hidayatullah et al. [10] more than 45 reactor designs are under development (46 including SLIMR). These include designs that are still in the conceptual phase, have detailed designs or designs from which prototype plants have been built. Not all 45 reactor designs will be discussed here, only the ones that are further in their development stage and the ones closest to the design of the SLIMR. For example, reactors cooled by liquid metal or gas are left out.

SSR

SMR designs using supercritical water are scarce. In fact, only one is mentioned in literature; the SuperSafe Reactor (SSR). It is a scaled version of the CANDU-SCWR proposed by the Atomic Energy of Canada Limited (AECL) and is still in its conceptual phase [29]. Besides the use of supercritical water as its coolant this reactor differs significantly from the SLIMR design. The fuel consists of 13 wt% PuO_2 and 8 wt% ThO_2. Heavy water is used as the moderator and is stored in the calandria vessel surrounding the fuel assemblies, at the bottom of the Reactor Pressure Vessel (RPV), see Figure 1.1. The coolant is at a pressure of 25 MPA and its temperature is expected to range from 350 °C at the inlet to 625 °C at the outlet. At a thermal power rating of 670 MW and an expected efficiency of 45% the reactor will be generating 300 MW of electrical power. Passive decay heat removal systems are in place, such that during severe accidents human intervention is unnecessary. The primary coolant loop takes away heat through natural circulation and the heavy water moderator acts as a heat sink and can even transport the decay heat away during Loss of Coolant Accident (LOCA) scenarios. [42]

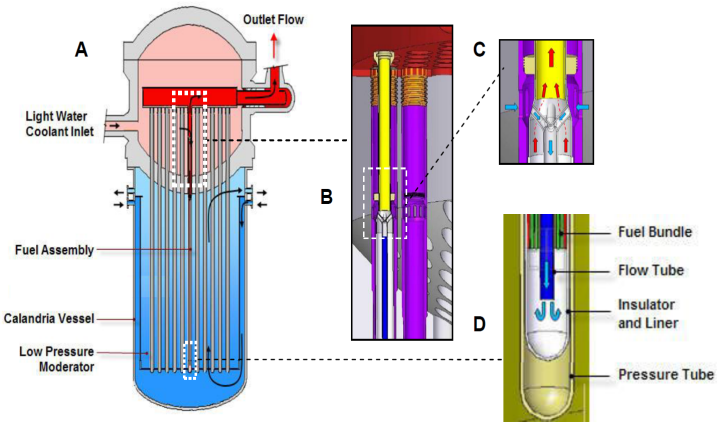

Figure 1.1: The SuperSafe Reactor. The blue color indicated the heavy water surrounding the calandria. Image adopted from Yetisir [42].

SMART

The Korean Atomic Research Institute has proposed a design for a small integral Pressurized Water Reactor (iPWR) with inherent and passive safety features. The reactor is scheduled to produce 330 MWth, which should provide 90 MW electrical energy and is able to desalinate 40,000 m^3/day [3]. The integral design of the reactor ensures that leakages are prevented, because all primary circuit components are contained within the RPV. After the design was completed a scaled version (1:5) of 65MW was constructed to test the performance and safety features of the design [4]. In March 2015 South Korea and Saudi Arabia signed a memorandum of understanding, in which agreement was made on studying the feasibility of building two South Korean-designed SMART reactors in Saudi Arabia within the near future [41].

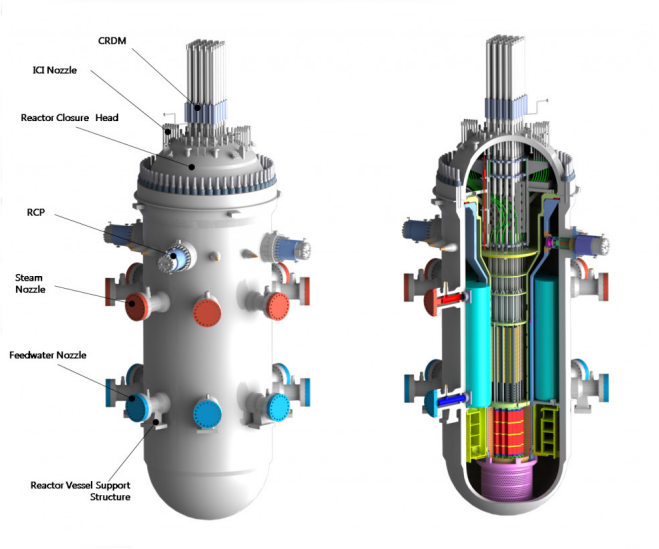

Figure 1.2: The SMART design. Image adopted from [1].

Westinghouse SMR

The Westinghouse Small Modular Reactor (WSMR) is one of the bigger SMRs. This iPWR, with an 800 MW thermal power capacity, is expected to generate 225 MWe. The design is similar to the Westinghouse AP1000 plant, but smaller. By using the same (proven) features and systems Westinghouse hopes to accelerate the licensing process. However, different from the AP1000 but similar to the SMART reactor, the whole reactor coolant system is incorporated into the RPV. Coolant flow is driven by eight pumps and in accident scenarios the reactor can passively remove its heat during the subsequent seven days [29]. Westinghouse sought to get funding for its light water reactor design, but failed to do so. In January 2014 Westinghouse shelved the project, because without government funding and a prospective sale of 30 to 50 units the project was not economical viable to pursue at that moment. So plans for its SMR are delayed, but small reactors are still kept on the agenda [40].

mPower

This reactor design by Babcock & Wilcox (B&W) was proposed in June 2009 and was planned to operate with a capacity of 125 MWe, but after pre-application activities with the U.S. Nuclear Regulatory Commission the rated capacity has been increased to 180 MWe [19]. This iPWR design holds all the components of the NSSS and control rods within its vessel to ensure LOCA scenarios are prevented. 'Off-the-shelf' balance of plant systems are used in the design, e.g. steam generators of older B&W designs have been improved and implemented in the mPower design [9]. The coolant is driven by pumps, but during accidents scenarios the reactor is able to cool itself passively by natural convection. The rather large RPV is 22 m high with a diameter of 4.5 m, but it is still small enough to be transported by rail or barge from the factory to the power plant site. At this site two to four modules can be placed in an underground

seismic I category containment to increase the power capacity of the power plant [22].

Where Westinghouse failed to receive funding, B&W succeeded in receiving funding for further development of its reactor design. The Department of Energy (DOE) of the U.S. called for applications for new light-water reactor designs in January 2012 and offered to allocate $452 million over five years to one or two designs. The mPower design of B&W was the first design to be funded by the DOE and its design has been further developed together with Bechtel and TVA. Although the DOE funded the project, expected was that industry investors would meet costs to at least the same amount as the DOE was spending [40]. However, these investors proved to be hard to find and while B&W continues to believe in its design they announced that its development program for the mPower design is being restructured as their spending is reduced to $15 million per year, due to lack of sufficient funding. Though, they still expect that a mid2020-timeframe for licensing and deploying is still possible [2].

NuScale

After the design of B&W, NuScale was the second design chosen to be funded by the DOE. NuScale Power signed a contract in May 2014, which stated that $217 million would be allocated over five years towards the development of the NuScale design. Again investors were expected to finance half of the costs of the project. NuScale Power expects that construction of a power plant could begin as soon as 2020 and that operation of the plant can start in 2023 [40].

The design of the NuScale can be compared to the SLIMR design regarding its simplicity and passive features. NuScale is a pressurized light-water reactor with a primary water loop flow driven by natural convection, generated by the density difference between the riser and the downcomer. Each module can produce up to 45 MWe and a single power plant facility can accommodate up to 12 modules. The RPV contains the reactor core, a 'first-of-a-kind' helical coil steam generator and the pressurizer. So an integral design is applied here as well. The reactor pressure vessel is 12.7 m high and 2.7 m in diameter, the total NSSS (including the containment vessel) is 24.6 m high and 4.6 m in diameter [22]. The systems has two emergency heat removal systems; Decay Heat Removal System (DHRS) and the Containment Heat Removal System (CHRS). The DHRS uses one of the two helical coil steam generator tubes to create a natural circulation flow, which is connected with the pool in which the whole NSSS is submerged, to cool down the reactor. The CHRS uses the containment surrounding the RPV to cool down the core passively. Reactor vent valves at the top of the RPV are opened so water from the RPV can turn into steam and escape the RPV, after which the steam condenses at the wall of the outer containment [11]. This condensed water flows down and is drawn back into the core within the RPV through the lower valves, see Figure 1.3. However, from literature it is not clear how these valves are being opened. If this has to be done by an operator with the use of electricity, this system is not completely passive as operator intervention is still required. The cooling down process after opening the valves however is completely passive.

Overview of SMRs

Table 1.1 gives an overview of the specifications of each type of reactor, compared to the SLIMR characteristics determined in this report. The LWRs have lower core outlet temperatures compared to the supercritical water reactors, with the SSR being at the top with 625 °C. Furthermore, only the NuScale and the SLIMR have natural circulation in the RPV to drive the flow. And what can be seen is that although the reactors are called small, the RPVs still tend to be quite large. Based on this table the SLIMR design has serious potential.

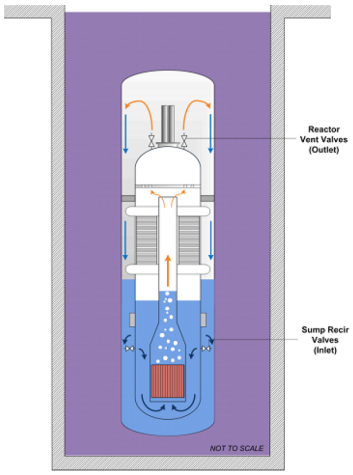

Figure 1.3: The CHRS system of the NuScale design. Image adopted from [22].

Table 1.1: Specifications of the mentioned SMRs.

Reactor design	**Power (MWe)**	**Type of fuel**	**Fuel assembly design**	**Size of RPV**	**Coolant**	**Circulation in RPV**	**Core outlet temperature** (°C)
SSR	300	13 wt% PuO_2 & 8 wt% ThO_2	78-element Canadian SCWR fuel assembly	D=∼4 m H=∼17 m	Supercritical water	Forced	625
SMART	90	<5 wt% UO_2	Standard LWR fuel in 17 x 17	D=5.3 m H=15.5 m	Light water	Forced	323
Westinghouse SMR	225	<5 wt% UO_2	17 x 17 RFA (designed by Westinghouse)	D=3.5 m H=24.7 m	Light water	Forced	310
mPower	180	<5 wt% UO_2	Standard LWR fuel in 17 x 17	D=4.5 m H=22 m	Light water	Forced	320
NuScale	45	<5 wt% UO_2	Standard LWR fuel in 17 x 17	D=2.7 m H=13.7 m	Light water	Natural	329
SLIMR	140[1]	5.6 wt% UO_2	HPLWR FA design without moderator box	D=3.2 m H=16.4 m	Supercritical water	Natural	396

[1] Based on an expected efficiency of 40% and a thermal power of 350 MW.

1.2 The SLIMR design

Rohde [27] of the department NERA of the Reactor Institute Delft proposed the SLIMR design with the goal to increase the safety and efficiency of a SMR. Key features of this design are its simplicity and the fact that the design is inherently safe. The latter meaning that in accident scenarios the reactor can passively cool down without the intervention of an operator. A schematic drawing of the SLIMR design is given in Figure 1.4. By eliminating the use of external piping and valves and placing the primary loop as a whole inside the reactor reduces the risk of LOCA. The integral RPV, with a vessel thickness of 37 cm, holds the reactor core with on top a riser, surrounded by an annular downcomer. The heat exchanger is placed inside the RPV as well and is connected to the turbine generator unit. The entire RPV is submerged in a pool of water, which functions as a heat sink during accident scenarios and transports heat away during nominal operation.

Inside the RPV, water at a supercritical pressure of 25 MPa flows into the core at the bottom of the RPV, heats up and surpasses the supercritical temperature of 374 °C. From the core supercritical water enters the riser and flows to the top, from which it flows then back downwards towards the inlet of the core, while giving off its heat to the steam generator. This entire process occurs without the use of active systems, such as pumps. The primary water loop is driven by natural convection, which eliminates the needs for pumps and thus making the system simpler and safer. Natural convection is mainly possible due to the use of the beneficial physical properties of supercritical water, which is elaborated on in the next two sections. The reactor is designed to operate at 150 MWth, which should heat the water up from 280 °C to 400 °C. The desired outlet temperature of 400 °C was unfortunately not reached in the work of Veling [36], as his parameter study showed that the core exit temperature did not surpass 374 °C.

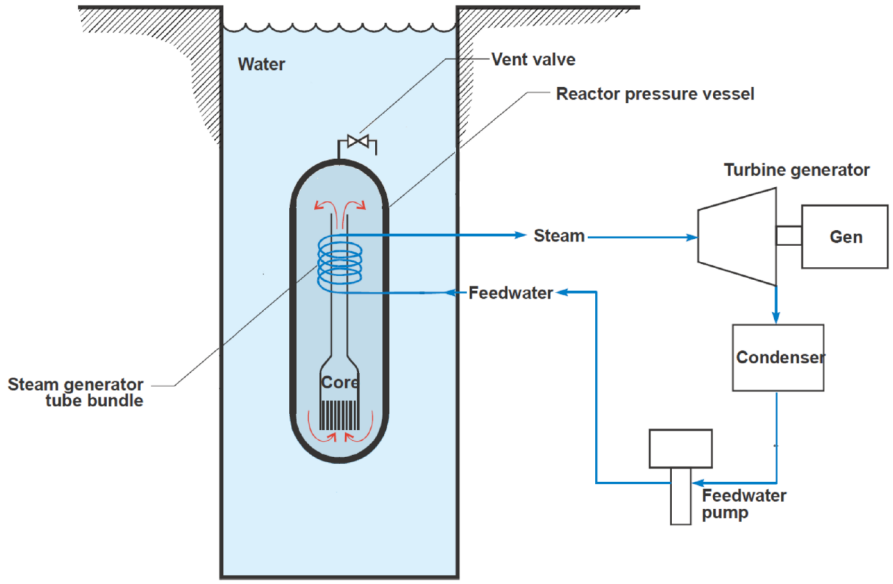

Figure 1.4: The SLIMR design as proposed by Veling [36]. Image adopted from [36].

1.2.1 Supercritical water

The use of supercritical water in the SLIMR design has two main purposes. In the first place reactors using supercritical water can reach higher temperatures than Light Water Reactors (LWRs). Light water reactors pressurize the water to increase the boiling temperature and thus increase their core exit temperature, but this can only go as far the supercritical temperature of 373.946 °C. By increasing the pressure above the supercritical pressure of 22.0640 MPa the water becomes supercritical instead of a vapor for higher temperatures and the density drop is less severe. Also the need for steam separators and dryers disappears when vapor is being avoided. Higher temperatures are beneficiary for the thermal efficiency of the steam turbine. As the Carnot cycle efficiency puts a theoretical limit on the efficiency of the steam turbine, the only way to increase the efficiency of a reactor is to increase its output temperature T_H, because the ambient temperature T_C is given, see Eq. 1.1. Supercritical water reactors can therefore reach efficiencies up to 44% in comparison with 34% for conventional LWRs [36]. [2]

$$\eta_{th} = 1 - \frac{T_C}{T_H} \tag{1.1}$$

Secondly, supercritical water has interesting properties that are beneficial for the operation of the reactor. There exists a point in the supercritical domain of water where properties vary strongly. This point is the pseudo-critical point and lies at 384.9 °C for a pressure of 25 MPa. At the pseudo-critical point the specific heat of water has a sharp peak, see Figure 1.5. This peak is beneficial for the operation of the reactor as a lot of heat can be absorbed in the water before its temperature starts to rise. Furthermore, as can be seen from Figure 1.5 the density decreases suddenly near the pseudo-critical point. This phenomenon is often compared with the phase change between the fluid and vapor state of water where even a bigger drop is noticeable. However, in this case there is no phase change and the density drops continuously over the entire temperature range of the reactor. This density drop is exploited in the reactor for its ability to drive the natural circulation in the water loop, elaborated more in the next section.

Though supercritical water has its benefits, to actually implement it in the design some challenges have to be overcome as well. For one, the supercritical water has a corrosive impact on many materials and with high pressures and high temperatures the materials in the reactor are under much strain[36]. Suitable materials have to be found to prevent damage of reactor components. Furthermore, as will be explained in section 2.2, the heat transfer from the fuel rods to the supercritical water can be deteriorated near the pseudo-critical point. As a result the heat from the fuel can not escape the fuel rods and the temperature of the fuel rods will increase rapidly; a highly unwanted situation which must be avoided by design.

1.2.2 Natural circulation

In the new generation III+ and generation IV designs engineers seek opportunities to minimize the use of active systems in the reactors. One way is by using natural circulation to drive the primary coolant and therefore limiting the need for pumps. Natural circulation occurs when in one part of the loop the coolant has a lower density than in the other part, see Figure 1.6. In the core at the lower part of the inner tube the primary coolant heats up and as a result its density decreases. The heat exchanger in the outer annulus extracts the heat from the coolant and the density increases. These two parts of the primary coolant loop thus have different densities and a gravitational pressure drop is introduced in the system. This gravitational pressure drop pushes the hot coolant in the inner tube upwards and drives down the cold coolant downwards.

[2] There are other ways to increase the efficiency of the power plant, by reducing friction losses in the steam turbine for example, however it can never exceed the Carnot cycle efficiency.

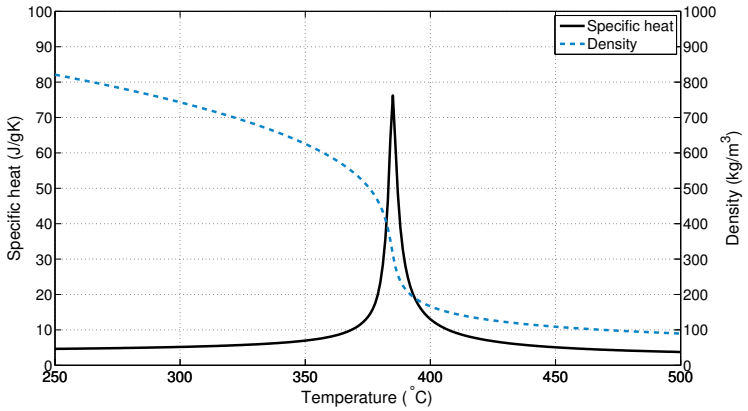

Figure 1.5: Specific heat and density of water versus temperature at a pressure of 25 MPa. The pseudo-critical point lies at the maximum of the specific heat. Data taken from NIST [6].

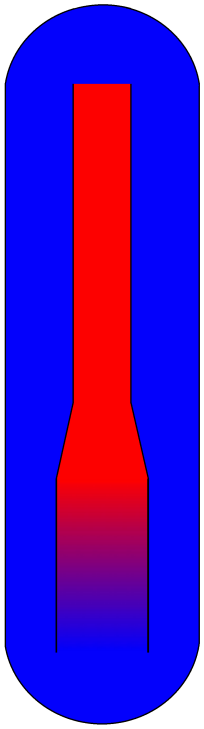

Figure 1.6: The relatively heavy cold water flows down and pushes the relative light hot water in the riser to the top.

The mass flow that is imposed by the process of natural circulation must be high enough to cool down the fuel rods inside the core and thus prevent excessive temperatures. For this reason a riser is put on top of the core to increase the gravitational pressure drop between the riser and the annular downcomer.

Furthermore, the gravitational pressure drop also depends on the density difference of the coolant between the two parts. In a Boiling Water Reactor (BWR) this density difference can become quite large as steam has a significant lower density than water as a fluid. Therefore this feature has been incorporated in one of the new generation III+ designs; the Economic Simplified Boiling Water Reactor (ESBWR). Its coolant flow is driven solely by natural circulation. The SLIMR design uses also natural circulation and becomes possible mainly due to the large density drop around the pseudo critical-point of supercritical water, see Figure 1.5. Without this density drop much higher temperatures would have to be reached to get a sufficient gravitational pressure drop. Also in the SLIMR design a riser is placed on top of the core to stimulate the natural circulation.

1.2.3 The core

In the previous work of Veling [36] the core of the SLIMR has been modeled as a single-pass core configuration, meaning that the coolant flows straight from the inlet to the outlet of the core. However, during his parameter study he found that it was impossible to meet two goals at the same time, which are; reaching high core exit temperatures and avoiding heat transfer deterioration. Heat transfer deterioration is when there is a significant decrease of the heat transfer coefficient between the fuel rods and the coolant. Whenever a high exit temperature is desirable, either the power has to increase or the mass flow has to be decreased to ensure enough heat to be transported to the coolant, at a fixed inlet temperature. In his single-pass core configuration this meant that heat transfer deterioration would come in play. For this reason an other core design is proposed in this thesis, specifically a smaller version of the three-pass core configuration of the HPLWR.

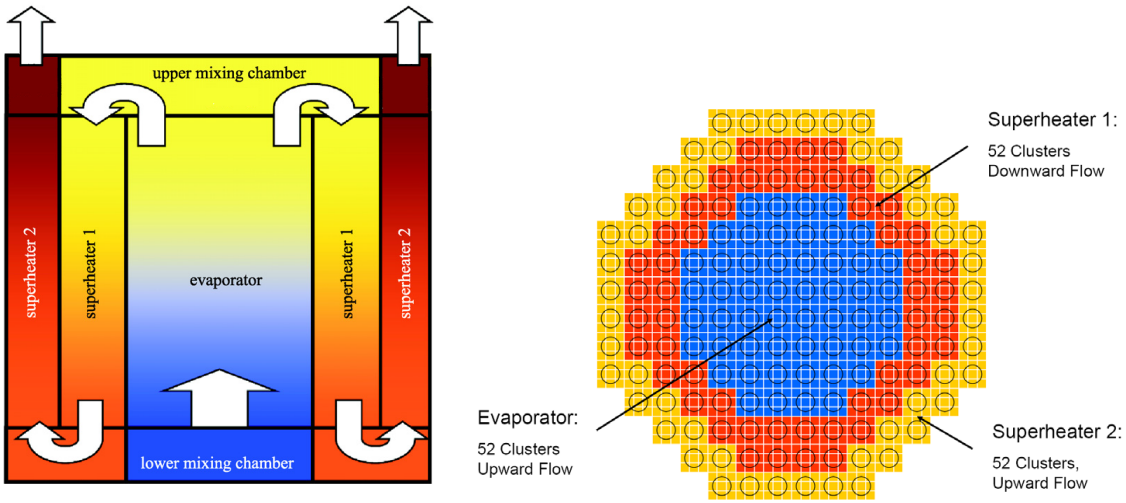

(a) Side view

(b) Cross sectional view

Figure 1.7: (a) Water heats up in three subsequent sections in the core. Image adopted from Schlagenhaufer et al. [30]. (b) Each ring consist of 52 clusters. Image adopted from Starflinger [32].

The HPLWR is a reactor design for a supercritical water reactor commissioned by the European Commission as a contribution to the Generation IV international forum (GIF). The HPLWR incorporates a three-pass core configuration as illustrated in Figure 1.7. To enhance the heat transfer the coolant flows through three sections in the core. The supercritical water enters the Evaporator at the bottom of the core

and flows upwards to the first mixing chamber. This mixing chamber makes sure the water enters the Superheater I homogeneously in temperature. The water flows then down to the second mixing chamber, after which it flows upward through the Superheater II and exits the core at the top into the riser. By incorporating this three-pass design the mass flux increases compared to the single-pass design and this enhances turbulence and with it the heat transfer from the fuel rods to the water. Also, it has been shown through computational models that the three-pass design is more thermal hydraulically stable compared to the single-pass design [32].

Furthermore, the radial averaged axial water density profile, $< \rho > (x)$, becomes less steep, due to the downward flow in the Superheater I and slightly flattens the power density profile through moderation. However, this effect is small, because most of the heat is dissipated in the Evaporator. The power ratio between the Evaporator, Superheater I and II is approximately 4:2:1 respectively, which means that the largest enthalpy step occurs in the Evaporator. To avoid high power densities in the lower part and low power densities in the upper part of the core the enrichment is varied in the axial direction. In the lower part the density of the water is higher, so the moderation of neutrons will be higher. Therefore the enrichment of the fuel is lower in the lower part of the core compared to the upper part of the core. Each ring consists of 52 fuel assembly clusters, where every cluster consists of nine fuel assemblies. The fuel assemblies consist each of 40 fuel rods surrounding a moderator box. The moderator box is used to even out the power profile in the axial direction, by pumping cold water through them. In some clusters these moderator boxes are used to guide control rods.

1.2.4 The stability problem

With the advent of nuclear reactors with natural circulation, e.g. the BWR Dodewaard reactor in the Netherlands, more research was done into the instabilities that occur in such two-phase systems. An unstable system is defined as when the system is perturbed and does not recover to its original steady state. Just as forced convection BWR's, natural circulation driven water loops are prone to instabilities in the system, because of the feedback mechanisms that are in play. These instabilities not only occur in two-phase systems, in which there is a clear boundary between the fluid and gas and large variations in thermophysical properties occur, but also in one-phase systems, such as the supercritical water reactors. Different types of instabilities have been identified at the time and can be roughly split into two categories; static and dynamic instabilities.

Static instabilities are sudden flow excursions that put the system in another operational point, see Figure 1.8(c). In this example the flow is perturbed and the mass flow rate increases to a higher value, where it stays at. These operational points seem to be stable, but can be set off by perturbations after which the system settles into another operational point. These type of instabilities are also called Ledinegg instabilities and occur in forced circulation water loops when the pressure versus mass flow characteristic of the pump intersects at multiple points with the pressure characteristic of the water loop [8]. However, the SLIMR does not have a forced circulation water loop. In this case Ledinegg instabilities occur when the gravitational pressure drop and the frictional pressure drop have more than one solution at the same operational point [17].

The second type of instabilities are of a more dynamic nature, under which Density Wave Oscillations are most common. Figure 1.8(b) shows an unstable system in which a perturbation is amplified over time and brings the system out of its steady state. A stable system would responds as in Figure 1.8(a), i.e. the perturbation dies out over time. The former one can damage the system and must be avoided at all times. An oscillating mass flow rate influences the density of the water leaving the core, because a water flow with a low mass flow rate heats up more and the density of the water will decrease. This

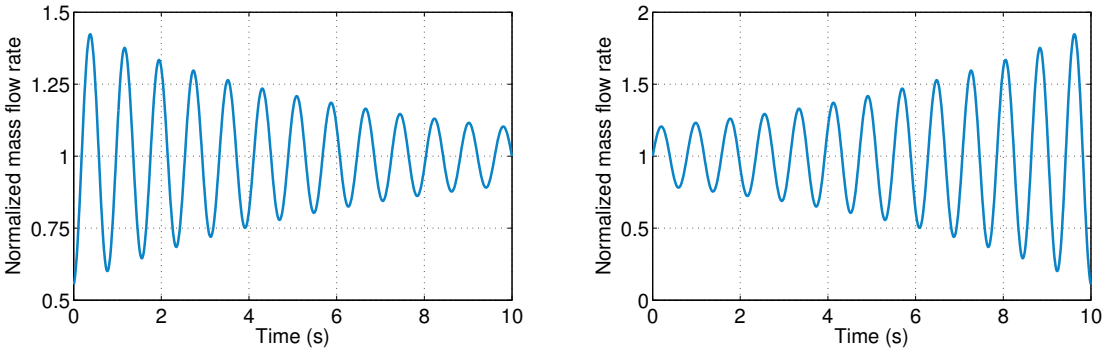

(a) A stable system

(b) An unstable system

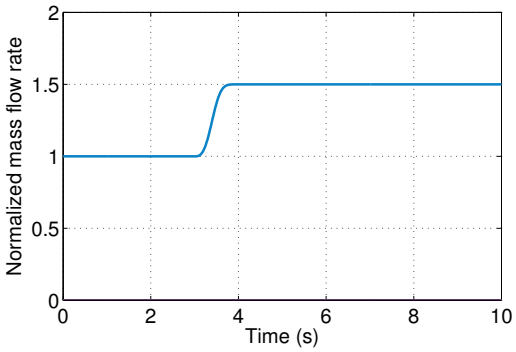

(c) Ledinegg instability

Figure 1.8: Examples of the different types of responses to perturbations in the system.

increases the mass flow rate, due to the greater density difference between the riser and the downcomer, after which the water heats up less in the core and the density at the core outlet increases. This time it lowers the density difference and decreases the mass flow rate, starting the same process all over again and introducing density waves throughout the water loop. If the perturbation grows in time, thus a decay ratio bigger than 1, the system is considered unstable. If the perturbation dies out, a decay ratio smaller than 1, the system is considered stable. [36]

Both type of instabilities can cause damage to the system, e.g. by extra stress on the materials, temperature changes that follow up quickly after each other and the presence of local heating spots due to deteriorated heat transfer. This thesis will therefore look into the behaviour of the system when perturbations are introduced.

1.3 Literature review

This literature review gives an overview of the research that has been done in this field of study. First a description is given of the work done by Veling [36], as this work is a continuation of the work done by him on the SLIMR design. Secondly, other research similar to this work is being discussed in the second subsection.

1.3.1 Thermal hydraulics of the SLIMR

Veling [36] investigated the feasibility of the SLIMR design by investigating if the reactor is able to operate inherently safe under normal and accidental situations. To this end Veling divided his research into four phases, which answered the following questions:

Phase A Is it possible to obtain a geometry in which the SLIMR has a safe nominal operation point, which is stable and in which no heat transfer deterioration occurs?

Phase B What is the steady-state heat loss of such a SLIMR design during normal operation?

Phase C With what pool dimensions is it possible to transfer this heat passively to the environment and maintain safe working conditions (i.e. a pool water temperature around 40 °C)?

Phase D Is it possible to obtain a geometry of the SLIMR design that is within the boundaries of a safe nominal operation and allows safe deposition of decay heat to the environment under accidental situations in a fully passive way, without damaging the core? [36]

To answer these questions Veling [36] developed a transient thermal hydraulic system-code for the SLIMR, based on the latest code for the DeLight-facility, which was developed over the years through the work of Koopman [16], Kam [15] and Spoelstra [31]. This code modeled the natural circulation flow inside the RPV and the heat transfer from the downcomer via the RPV wall to the pool in one dimension. The heat transfer mechanisms inside the pool where modeled with a single node representing the pool.

For phase A different geometry parameters where varied to investigate the stability of the flow, i.e. the riser diameter, the outer diameter of the downcomer, the riser length, the core height, the core inlet friction, the core inlet temperature and the core power. In this parameter research no thermal hydraulic instabilities were found for the range of the parameters. Remarkable was that the core exit temperature did not exceed 374 °C, meaning that the pseudo-critical point is not reached resulting in a low thermal efficiency.

For phase B the heat loss to the pool was studied by varying geometry parameters of the RPV. It was found that the heat loss was significant and lies in the order of 1 MW. This heat loss during nominal operation decreases the thermal efficiency, but during a SCRAM situation enables the reactor to passively remove heat. Veling [36] recommended that this problem should be addressed in further research.

For phase C Veling [36] investigated the required dimensions of the pool to passively remove heat received from the RPV to the environment. As the main mechanism of heat removal of the pool is by evaporation from the free surface of the pool, the heat removal scaled with the area of the free surface. Veling [36] found that a free pool surface of 1600 m^2 is required to maintain the pool temperature around 40 °C, which is very large. After careful validating his code, this was found not to be correct and the surface or pool temperature could be lowered.

Finally, for phase D Veling [36] found that the reactor is able to cool down passively during SCRAM situations only when the temperature of the coolant does not exceed the pseudo-critical temperature, 385 °C. When the coolant temperature surpasses the pseudo-critical point, the temperature rapidly increases towards the design limits of the reactor. The heat sink capacity in the RPV decreases significantly after the pseudo-critical point, because the density (and thus amount of water inside the reactor) and the specific heat capacity of the water decrease both (Figure 1.5). This results in a rapid temperature increase.

1.3.2 Other research

This literature review gives an overview of similar work in this field of study. The main focus lies on work that includes neutronic-thermalhydraulic coupling.

For studying a new design of a pebble bed high-temperature reactor module (HTR-PM) Dong et al. [5] developed a nodal neutron kinetics model. As they argue, the ratio of height to diameter of the core is larger than former designs, so the point kinetics model would be unfit for control system design and verification. The reactor core of the HTR-PM has been divided into ten axial nodes to better describe the distributed information in the core, i.e. the power distribution. This code has been coupled to a thermal hydraulics code, which as a whole showed good numerical simulation results for the static precision as well as transient response in the system. The developed nodal kinetic model has been used as a guideline in this research.

Other work involving coupling of the neutronics and thermal hydraulics was done for the High Performance Light Water Reactor (HPLWR), a reactor design closely related to the SLIMR, by T. Reiss et al. [26]. They developed a coupled neutronics-thermalhydraulics program system to determine the steady-state parameters of the HPLWR while taking burn up into account as well. This program consists of three modules; a Monte Carlo N-Particle (MCNP) module, which calculates the power distribution for a specific core setup; a thermal hydraulics module, which calculates the temperature and density distributions of the system with the use of conservations and heat transfer laws; a coupling module, which gives the default values, handles the communication between the other two modules and evaluates the outcome. This program was used to study the effect of modifying the axial enrichment profile, moderator box and water gap percentages to optimise the power distribution in the core. Also Waata [39] developed a coupled code system to investigate the HPLWR, a proposed fuel assembly for the HPLWR to be more specific. She coupled the MCNP code and the sub-channel code STAFAS (Sub-channel Thermal-hydraulics Analysis of a Fuel Assembly under Supercritical conditions). The STAFAS code handles supercritical properties of the coolant as well as separate moderator channels. The coupled system calculates power and temperature profiles of the system until convergence is reached. Coupling and decoupling showed significant different results for the power distribution. Furthermore, the code can be used to study design modifications in the enrichment of fuel rods and enhanced mixing by grid spacers for the HPLWR.

Furthermore, Schlagenhaufer et al. [30] studied the passive and active reactivity control mechanisms for HPLWR fuel assemblies (including moderator boxes) with the use of the MCNP5 code. Passive reactivity control mechanisms such as the reactivity feedback of the moderator density and reactivity feedback of the fuel temperature, i.e. Doppler effect. Active reactivity control mechanism involved reactivity changes as a result of control rods. It was found that the reactivity coefficients for the moderator density were positive and for the fuel temperature were negative, as is required for safe operations as these ensure that feedback mechanisms are negative. These results are used as a benchmark for the reactivity feedback coefficients found in this research, for HPLWR fuel assemblies without moderator boxes.

Next to computational modelling, experiments have also been done to study the stability of supercritical

water based reactors. Specifically, Rohde et al. [28] designed an experimental facility, called DeLight, which was built afterwards by the department NERA of the Reactor Institute Delft. Subsequently, T'Joen and Rohde [33] studied the stability regime of the DeLight facility, to study a natural circulation driven HPLWR. The DeLight facility is a scaled model using Freon R23 as a coolant, because its supercritical properties are reached at lower pressures and temperatures with respect to water, making the experiments easier and safer to perform. The experimental setup uses electric heaters to heat up the Freon R23 and therefore an artificial neutronic feedback had to be included. This neutronic feedback was based on the 6 group point kinetics equations, the average density in the heated section and the moderator density feedback coefficients found in Schlagenhaufer et al. [30]. Without neutronic feedback in the setup no instabilities were found, but with neutronic-thermalhydraulic coupling instabilities were found. This is interesting as it shows the importance of neutronic-thermalhydraulic coupling in studying natural circulations loops, which is the main aim of this research.

1.4 Aim and structure of this thesis

Due to this research being a follow up on the study Veling [36] did on the SLIMR design, the aim of this research is rather similar to Veling's research. However, Veling took into account the heat transfer from the natural circulated flow through the RPV to the surrounding pool. The focus in this research is directed more towards the processes inside the RPV. Building upon Veling's work this research replaces the one-pass core for a three-pass core configuration to improve the performance of the reactor. Secondly, Veling only examined the thermal hydraulics of the SLIMR design, excluding the neutronics inside the core. This research will include the neutronics and the accompanying feedback mechanisms to study the stability of the design.

To this end this research will try to find an answer to the following main research question:

"***How can the SLIMR design be made feasible, while meeting performance and stability standards?***"

The SLIMR design has not been found infeasible by Veling [36], nevertheless the design can be improved on its performance and the impact of the neutronics on the stability of the reactor can be investigated. To better serve the answering of this question, three sub-questions are asked. These questions are:

1. What are optimal design parameters to increase the performance of the SLIMR including the three-pass core configuration?
2. How can the small reactor core be made critical under supercritical conditions?
3. How does the coupling of the thermal hydraulics and the neutronics have an effect on the stability of the SLIMR?

So first the performance of the reactor, including the proposed three-pass core configuration, will be studied by performing a parameter study with the updated SLIMR model. When the most suitable design parameters are chosen the small core will be examined on its characteristics to find out if it can be made critical with supercritical water as its moderator. Also the reactivity feedback coefficients of the core are determined. This will be done by Monte-Carlo calculations, with the use of the program *Serpent* (V2.1.12) [18]. Subsequently, a stability analysis is performed by coupling a nodal kinetics model with the thermal hydraulics model for the SLIMR, using reactivity feedback coefficients found by *Serpent* [18].

The structure of this thesis is as follows. Chapter 2 describes the problem of heat transfer deterioration and works out the nodal kinetics equations and the feedback mechanisms. Chapter 3 introduces the numerical model and the coupling of the thermal hydraulics code and the nodal kinetics model.

Chapter 4 reviews the results and answers the three sub-questions. Finally, Chapter 5 answers the main research question, discusses the methodology of the work and gives recommendations for future work. The nomenclature and the explanation of abbreviations are given in the beginning of this document for easy access.

Chapter 2

Theory

This section covers the theory used in expanding the SLIMR model. First the proposed three-pass core configuration is described, after which the problem of heat transfer deterioration is explained. Subsequently, the reactivity feedback mechanisms which are being modelled are described followed by the derivation of the nodal kinetics model and the energy conservation equation over the fuel pins.

2.1 The proposal for a three-pass core configuration

The proposal for the SLIMR is to benefit from the HPLWR findings and, hence, it is proposed to incorporate a similar but smaller version of the HPLWR three-pass core configuration. This configuration is illustrated in Figure 2.1(a) where every square represents a fuel assembly instead of a fuel assembly cluster. The SLIMR Evaporator consists of 57 fuel assemblies, and the Superheaters both consists of 64 fuel assemblies. The core has an equivalent diameter of 1.37 m and a height of 4.2 m, similar as the core design of Veling [36]. The fuel assemblies however lack a moderator box[1], instead each fuel assembly consists of 49 fuel rods, see Figure 2.1(b). The main reason for incorporating the three-pass core design is to deal with the heat transfer deterioration by relying on the research done for the HPLWR core. And by using a three-pass core design the friction in the loop increases and lowers the mass flow rate. Thus the three-pass core configuration ensures the water heats up more gradually, compared with the single-pass configuration, and it is able to reach higher core outlet temperatures to increase the efficiency and exploit the benefits associated with surpassing the pseudo-critical point. In the next section the heat transfer associated with this design is further explained.

[1] The moderator box is not included in the design as it increases the complexity of the model and requires a counter-flow driven by pumps.

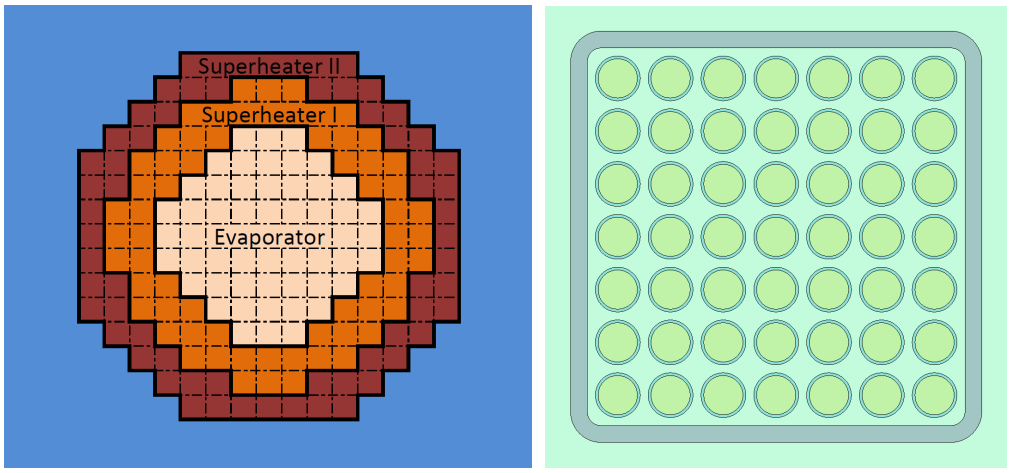

(a) SLIMR core configuration.

(b) A fuel assembly consisting of 49 fuel rods surrounded by the fuel assembly wall. Each fuel rod is surrounded by a 0.5mm thick cladding.

Figure 2.1: The proposed core configuration for the SLIMR design.

2.2 Heat transfer deterioration

Increasing the efficiency of the reactor is the main reason why supercritical water is being used, as higher temperatures can be reached. However, with the use of supercritical water a phenomenon called Heat Transfer Deterioration (HTD) can occur. Around the pseudo-critical point physical properties vary strongly and can cause a significant decrease of the heat transfer coefficient between the wall and the coolant. This phenomenon can occur locally and has as a consequence that the wall temperature at that specific location increases rapidly, an unfavourable outcome as it imposes strain on the materials over time. This phenomenon can be compared to the Critical Heat Flux (CHF) in boiling water reactors, where a dry patch (due to vaporisation of the water) behaves as an insulating layer that limits the heat transfer. [32]

According to Jackson [13] HTD is especially present in flow structures with upward flow. He argues that HTD is caused by a reduction in turbulent diffusivity, because as the water heats up the low density wall layer becomes thicker and reduces the shear stress of the wall on the fluid. With higher shear stress more energy is fed into the turbulence, but with decreasing shear stress turbulence will decrease and this results in a less effective heat transfer. Furthermore, as the density becomes lower a buoyant layer exists at the wall surface and flattens the velocity profile in the radial direction of the tube. These two effects contribute to the process of laminarisation. In this laminarisation process the heat transfer coefficients take on lower values that are more representable for laminar flow conditions. [13]

During the design of a supercritical water reactor this phenomenon has to be taken into account. For this reason, Veling [36] used two criteria found through experiments by Vikhrev et al. [37] [38], as mentioned by Pioro & Duffey [24]. It was first found that HTD at the entrance of a vertical circular tube can be avoided if the ratio of the length and the diameter of the tube is set bigger than 40-60 ($L/D > 40-60$). Furthermore, HTD can be avoided at any section of the circular tube if the ratio of the heat flux and the mass flux in the tube is smaller than 0.4 kJ/kg ($q''/G < 0.4\ kJ/kg$). So in general,

HTD occurs in regions with high heat fluxes and/or low mass fluxes. In the research of Veling [36] these criteria were met and occurrences of HTD were assumed to be avoided. However, in his research he used a constant power density profile for the core of the reactor and by doing so he underestimated the actual heat flux at certain points in the reactor. In general the heat flux is high in the middle section and low at the outer sections of the core. Also the mass flux in his reactor was rather high, which enabled him to avoid HTD, but limit the performance of the reactor. In his SLIMR design the outlet temperature of the core did not reach the desired temperature of 400 °C and therefore the efficiency of the reactor is decreased. New calculations with a more realistic power distribution and lower mass flux (to increase outlet temperature) showed that the value of q''/G surpassed the value of 0.4 kJ/kg significantly.

To tackle this problem in the new design of the SLIMR these criteria are not taken into account, because for one, these criteria were found for a vertical circular tube. In the core design of the SLIMR a rod bundle structure is implemented with fuel assembly walls, so it is hard to say if these criteria apply to the SLIMR design as well. Secondly, there are measures that can be taken to avoid HTD at high heat fluxes and low mass fluxes. So in this case, also due to the fact that there exists a big gap in literature referring to HTD in these type of structures, a different approach is taken. By basing the core design of the SLIMR on the core design of the HPLWR it is assumed that HTD does not occur. The HPLWR is also exposed to the risk of HTD and measures have been taken to avoid HTD, proven by computational models. For example, the mixing chambers between the Evaporator and the Superheaters make sure that when the coolant re-enters the core no boundary layers exist at the entrance. Furthermore, fuel rods with a helical wire wrapped around them also prevent the occurrence of HTD [32]. The wrapped wire increases the turbulence by introducing an additional rotation component to the flow around the rod and by doing so it increases the heat transfer coefficient along the whole axis of the fuel rod [32]. Thus, by designing the core of the SLIMR similar to the one of the HPLWR it is assumed that HTD does not occur.

2.3 Feedback mechanisms

The feedback mechanisms that are included in the coupling between the neutronics and the thermal hydraulics are the Doppler feedback and the moderator density feedback. For boiling water reactors the fuel temperature coefficient, the moderator temperature coefficient and the coolant void coefficient are important parameters [23]. However, for a supercritical water reactor there are no voids, but there are strong variations in the density near the pseudo-critical point. Instead of the void fraction the moderator density coefficient is used for the reactivity feedback regarding changes in the moderator density. The moderator temperature coefficient is neglected as it is assumed that the moderator density has a bigger influence. The two feedback mechanisms, which are implemented in the SLIMR model, are explained next. The SLIMR model as used by Veling [36] is described in Section 3.3.1.

2.3.1 Doppler effect

The Doppler effect, also known as Doppler broadening, refers to the increased neutron absorption in fissionable material such as U^{238}, when the temperature of the fuel increases. This feedback mechanism contributes to one of the inherently safe processes in a reactor. While fast neutrons slow down towards the thermal region by scattering, they cross an energy spectrum in which i.e. the absorption cross section U^{238} has many resonance peaks. In these resonance peaks the cross section for absorbing a neutron is large, but it has a small energy width, see Figure 2.2. Whenever a neutron is absorbed by the fissionable material it can not cause another fission event, therefore decreasing the multiplication factor. When the temperature of the fuel increases these resonance peaks become broader and flatter, because the thermal motion of the heavy nuclei increases with temperature. The thermal motion of the heavy nuclei increases

the range of relative energies between the neutron and the nuclei for which the cross section is large, and neutrons with a slightly different energy before now fall into these broadened resonance peaks.

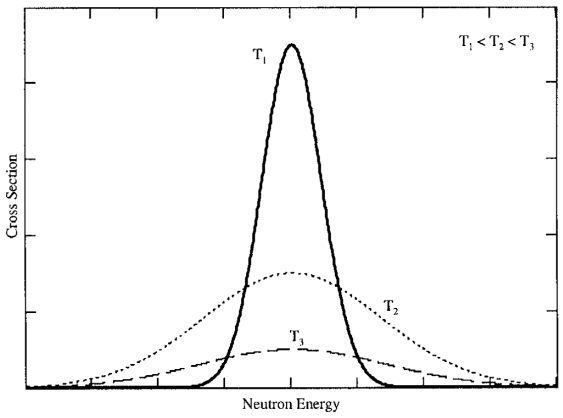

Figure 2.2: Illustration of the Doppler effect, for higher temperatures the resonance peak broadens and becomes lower. Image adopted from Jevremovic [14].

The Doppler effect therefore has a negative feedback on the reactivity for fuels containing e.g. U^{238}. When the power of the core increases through a positive reactivity insertion the temperature of the fuel will increase immediately. The Doppler effect takes place and reduces the resonance escape probability and decreases the reactivity, effectively decreasing the power of the core. For nuclear reactors to operate safely, the fuel temperature coefficient for the reactivity therefore has to be negative.

2.3.2 Moderator density feedback

Another feedback mechanism, especially present in super critical water reactors, is the moderator density feedback. The moderator in a reactor has the task to slow down the fast neutrons by scattering. When neutrons enter the thermal region fission events are possible and they can sustain the chain reaction. The density of the moderator fluid is important for the moderating power as the macroscopic cross section for scattering decreases when the moderator density decreases as well. So in case of a power increase more heat is dissipated to the moderator and the density decreases, decreasing the moderator power. Subsequently, fast neutrons are slowed down less and do not induce another fission event, thereby decreasing the power of the reactor. Thus, the moderator density coefficient for the reactivity should be positive for a nuclear reactor to operate inherently safe. For super critical water reactors this feedback coefficient plays an important role as the density of the water drops significantly when the pseudo-critical point is passed. In contrast with the fuel temperature feedback, this feedback mechanism has a small delay. The fuel temperature increases instantaneously when power is increased, but for the density of the moderator to decrease a small time has to pass as the heat transfer from the fuel to the moderator has a delay with respect to the core power.

2.4 Nodal kinetics

One of the aims of this research is to improve the SLIMR model, and this includes incorporating a realistic power distribution and the feedback mechanisms with respect to power. To this end neutronics have to be

included in the code and thus a set of equations is necessary to describe neutron behaviour in the core of the reactor. The thermal hydraulic code of Veling [36] for the SLIMR design is a 1-dimensional transient model and the equations describing the neutronics should be coherent with the thermal hydraulics model, while still enabling a quick calculation time. Therefore, e.g. a full 3-dimensional energy dependent neutronic code would be too comprehensive and unnecessary detailed for the purpose of this research. On the other hand the point kinetics equations would be unsufficient, because the core would then be modeled as a single point, while the thermal hydraulic code models the core with several nodes. A suitable neutronic model was found in the article written by Dong et al. [5]. In this research the core of a Modular High-Temperature Gas-cooled nuclear Reactor (MHTGR) is divided in ten axial nodes and for each node the point kinetics equations are derived. These nodal neutron kinetic equations are similar to the point kinetics equations, but then the neutron density is calculated in each node of the core and the nodes exchange neutrons through diffusion. The derivation as done by Dong et al. [5] is presented here and adjusted towards the case of the three-pass core design of the SLIMR. Although the thermal hydraulics model is 1-dimensional, this nodal kinetics model becomes a rough 2-dimensional model due to the three pass core design. Nodes not only exchange neutrons with neighbouring axial nodes, but also with neighbouring radial nodes in the Evaporator, Superheater I and Superheater II.

In the article of Dong et al. [5] the one energy-group diffusion equation is used as a starting point, which is for now still dependent on space.

$$\begin{cases} \dfrac{1}{v}\dfrac{\partial \phi_i(\mathbf{r},t)}{\partial t} = D\nabla^2\phi_i(\mathbf{r},t) - \Sigma_{a,i}\phi_i(\mathbf{r},t) + (1-\beta)\nu\Sigma_{f,i}\phi_i(\mathbf{r},t) + \displaystyle\sum_{k=1}^{6}\lambda_k C_{k,i}(\mathbf{r},t) \\ \dfrac{\partial C_{k,i}(\mathbf{r},t)}{\partial t} = \beta_k\,\nu\Sigma_{f,i}\phi_i(\mathbf{r},t) - \lambda_k C_{k,i}(\mathbf{r},t) \quad \text{with } k = 1\ldots6 \end{cases} \tag{2.1}$$

In these equations ϕ_i represents the space dependent neutron flux density, $C_{k,i}$ is the precursor density of the k^{th} delayed neutron group in the i^{th} node, D is the diffusion coefficient, v is the speed of thermal neutrons, ν is the neutron yield, β is the fraction of all the delayed fission neutrons, β_k is the fraction of the k^{th} delayed neutron family, λ_k is the decay constant of the k^{th} precursor group and $\Sigma_{f,i}$ and $\Sigma_{a,i}$ are respectively the macroscopic fission and absorption cross sections in the i^{th} node.

Integrating over space and dividing by the volume of the node gives the average value of each node:

$$\begin{cases} \dfrac{1}{v}\dfrac{\mathrm{d}\phi_i(t)}{\mathrm{d}t} = \Gamma_i(t) - \Sigma_{a,i}\phi_i(t) + (1-\beta)\nu\Sigma_{f,i}\phi_i(t) + \displaystyle\sum_{k=1}^{6}\lambda_k C_{k,i}(t) \\ \dfrac{\mathrm{d}C_{k,i}(t)}{\mathrm{d}t} = \beta_k\,\nu\Sigma_{f,i}\phi_i(t) - \lambda_k C_{k,i}(t) \quad \text{with } k = 1\ldots6 \end{cases} \tag{2.2}$$

The new variables are giving as follows:

$$\phi_i(t) = \frac{1}{V_i}\int_{V_i}\phi_i(\mathbf{r},t)\mathrm{d}\mathbf{r}^3 \tag{2.3}$$

$$C_{k,i}(t) = \frac{1}{V_i}\int_{V_i} C_{k,i}(\mathbf{r},t)\mathrm{d}\mathbf{r}^3 \tag{2.4}$$

$$\Gamma_i(t) = \frac{D}{V_i} \int_{V_i} \nabla^2 \phi_i(\mathbf{r}, t) \mathrm{d}\mathbf{r}^3 \tag{2.5}$$

The cyclic integral in Eq. 2.5 can be transformed into an integral over the surface of the specific node using the Gauss formula:

$$\begin{aligned} \Gamma_i(t) &= \frac{D}{V_i} \int_{V_i} \nabla^2 \phi_i(\mathbf{r}, t) \mathrm{d}\mathbf{r}^3 \\ &= \frac{D}{V_i} \oiint_{S_i} \langle \nabla \phi_i(\mathbf{r}, t), \mathbf{n}_i(\mathbf{r}) \rangle \mathrm{d}s \\ &\approx \sum_{j=1}^{N_i} \frac{DA_{ij}}{V_i d_{ij}} \left[\phi_j(t) - \phi_i(t) \right] \quad \text{with } j \text{ indicating adjacent nodes} \end{aligned} \tag{2.6}$$

In this equation the area of the interface between node i and adjacent node j is presented by A_{ij}, d_{ij} is the distance between the centers of node i and adjacent node j, N_i is the number of adjacent nodes of node i (including neighbouring axial ánd radial nodes), and $\mathbf{n}_i$ is the unit normal vector of the interface between node i and adjacent node j. Now by defining $\phi_i(t) = \nu n_i(t)$, where n is the neutron density, and substituting it together with Eq. 2.6 into Eq. 2.2 the following is obtained:

$$\begin{cases} \dfrac{\mathrm{d}n_i(t)}{\mathrm{d}t} = \left[(1-\beta) \dfrac{\nu\Sigma_{f,i}}{\Sigma_{a,i}} - 1 \right] \nu\Sigma_{a,i} n_i(t) + \displaystyle\sum_{j=1}^{N_i} \frac{DA_{ij}\nu}{V_i d_{ij}} \left[n_j(t) - n_i(t) \right] + \sum_{k=1}^{6} \lambda_k C_{k,i}(t) \\ \dfrac{\mathrm{d}C_{k,i}(t)}{\mathrm{d}t} = \beta_k \nu\Sigma_{f,i} \nu n_i(t) - \lambda_k C_{k,i}(t) \quad \text{with } k = 1 \ldots 6 \end{cases} \tag{2.7}$$

These equations can be further simplified if the multiplication factor, k_i, and the neutron life time, l_i, are substituted into the equations. These are defined as:

$$k_i = \frac{\nu\Sigma_{f,i}}{\Sigma_{a,i}} \tag{2.8}$$

$$l_i = \frac{1}{\nu\Sigma_{a,i}} \tag{2.9}$$

And substituting these into Eq. 2.7 yields:

$$\begin{cases} \dfrac{\mathrm{d}n_i(t)}{\mathrm{d}t} = \left[(1-\beta)k_i - 1 \right] \dfrac{1}{l_i} n_i(t) + \dfrac{1}{l_i} \displaystyle\sum_{j=1}^{N_i} \frac{DA_{ij}}{V_i d_{ij} \Sigma_{a,i}} \left[n_j(t) - n_i(t) \right] + \sum_{k=1}^{6} \lambda_k C_{k,i}(t) \\ \dfrac{\mathrm{d}C_{k,i}(t)}{\mathrm{d}t} = \dfrac{\beta_k}{l_i} k_i n_i(t) - \lambda_k C_{k,i}(t) \quad \text{with } k = 1 \ldots 6 \end{cases} \tag{2.10}$$

Finally the reactivity, ρ_i, and the mean generation time, Λ_i, are introduced:

$$\rho_i = \frac{k_i - 1}{k_i} \tag{2.11}$$

$$\Lambda_i = \frac{l_i}{k_i} \tag{2.12}$$

And these are substituted in Eq. 2.10:

$$\begin{cases} \dfrac{\mathrm{d}n_i(t)}{\mathrm{d}t} = \dfrac{\rho_i - \beta}{\Lambda_i} n_i(t) + \dfrac{1}{\Lambda_i} \displaystyle\sum_{j=1}^{N_i} \frac{DA_{ij}}{V_i d_{ij} k_i \Sigma_{a,i}} \big[n_j(t) - n_i(t) \big] + \sum_{k=1}^{6} \lambda_k C_{k,i}(t) \\ \dfrac{\mathrm{d}C_{k,i}(t)}{\mathrm{d}t} = \dfrac{\beta_k}{\Lambda_i} n_i(t) - \lambda_k C_{k,i}(t) \quad \text{with } k = 1 \ldots 6 \end{cases} \tag{2.13}$$

One final step includes cleaning up the equation and introducing the relative neutron and precursor density. The relative neutron and precursor density are defined as following, respectively; $n_{r,i} = n_i / n_{i,0}$ and $C_{r,k,i} = C_{k,i} / C_{k,i0}$. In these definitions $n_{i,0}$ and $C_{k,i0}$ are the neutron and precursor densities in steady state conditions respectively and the index r indicates the relative value. And from Eq. 2.10 it follows that during steady state, in which the time derivative equals zero, these are related with the next equation:

$$n_{i0} = \frac{\lambda_k l_i}{\beta_k k_i} C_{i,k0} \tag{2.14}$$

Cleaning up the equations involves splitting the diffusion term into two terms with the coupling coefficients, $\xi_{i,i}$ and $\xi_{i,j}$. Substituting these coupling coefficients, Eq. 2.14 and the relative neutron and precursor density gives:

$$\begin{cases} \dfrac{\mathrm{d}n_{r,i}(t)}{\mathrm{d}t} = \dfrac{\rho_i - \beta - \xi_{i,i}}{\Lambda_i} n_{r,i}(t) + \dfrac{1}{\Lambda_i} \displaystyle\sum_{j=1}^{N_i} \xi_{i,j} n_{r,j}(t) + \sum_{k=1}^{6} \lambda_k C_{r,k,i}(t) \\ \dfrac{\mathrm{d}C_{r,k,i}(t)}{\mathrm{d}t} = \lambda_k \big(n_{r,i}(t) - C_{r,k,i}(t) \big) \quad \text{with } k = 1 \ldots 6 \end{cases} \tag{2.15}$$

in which:

$$\xi_{i,i} = \sum_{j=1}^{N_i} \frac{DA_{ij}}{\nu \Sigma_{f,i} V_i d_{ij}} \tag{2.16}$$

$$\xi_{i,j} = \left(\frac{n_{j0}}{n_{i0}} \right) \frac{DA_{ij}}{\nu \Sigma_{f,i} V_i d_{ij}} \tag{2.17}$$

In Eq. 2.16 the summation is over all neighbouring nodes, so N_i equals the number of nodes adjacent to the i^{th} node. With Eq. 2.15 the nodal kinetics model is complete and will be used in the SLIMR model. For every node the neutron density can be calculated and the power distribution accordingly, because the power scales with the neutron density, see Eq. 2.18.

$$P_i(t) = w_f \Sigma_f \nu n_i(t) \tag{2.18}$$

w_f is the energy released during a fission event. The power in every node can now be calculated using the relative neutron density and the steady state neutron density. The latter one is calculated with the Monte-Carlo code *Serpent* [18] in this research, but it can be calculated with other reactor physics calculation codes (either stochastic as in this research or deterministic depending on the method and accuracy).

2.5 Fuel temperature

Incorporating the two feedback mechanisms mentioned in the SLIMR model requires calculating the density of the moderator and the temperature of the fuel. In the SLIMR model of Veling [36] the enthalpy of the coolant/moderator in every node is calculated and using splines the density can be calculated. However, the fuel temperature is not calculated in each node and again a relationship is necessary that matches the SLIMR model in its accuracy and computational time. For this reason a straight forward energy conservation equation is set up over a single fuel rod in each node to calculate the average temperature of the fuel rod. This enables quick calculations in contrast with a radial temperature dependent approach, which would require more computational time. The energy conservation equation over the fuel rod is presented next and includes the power generated by the fuel, heat conduction to adjacent fuel rod elements and heat conduction towards the moderator. Radiation is not taken into account.

$$\rho c_p \frac{\partial T_f}{\partial t} = q'''_{core} + \lambda_f \nabla^2 T_f - q'''_{f\to m} \tag{2.19}$$

In this equation T_f is the temperature of the fuel, ρ and c_p are the density and specific heat of UO_2 respectively, q'''_{core} is the volumetric heating rate, λ_f is the thermal conductivity of UO_2 and $q'''_{f\to m}$ is the heat loss from the fuel to the coolant. To be consistent, just as in Section 2.4, this equation will be discretized in space. The temporal discretization will be handled in the next chapter. The discretization in space involves integrating over the volume of each fuel rod element while considering only axial dependence of the fuel rod's temperature.

$$\begin{aligned}
\rho c_p \int_{V_i} \frac{\partial T_f}{\partial t} \mathrm{d}\mathbf{r}^3 &= \int_{V_i} q'''_{core} \mathrm{d}\mathbf{r}^3 + \int_{V_i} \lambda_f \nabla^2 T_f \,\mathrm{d}\mathbf{r}^3 - \int_{V_i} q'''_{f\to m} \mathrm{d}\mathbf{r}^3 \\
\rho c_p V_i \frac{\mathrm{d}T_{f,i}}{\mathrm{d}t} &= P_{rod,i} + \int_{A_i} \int_{z_{i-\frac{1}{2}}}^{z_{i+\frac{1}{2}}} \lambda_f \frac{\partial^2 T_f}{\partial z^2} \mathrm{d}z \mathrm{d}A + A_{cyl} h (T_{m,i} - T_{f,i}) \\
\rho c_p V_i \frac{\mathrm{d}T_{f,i}}{\mathrm{d}t} &= P_{rod,i} + \frac{\pi D_{rod}^2}{4} \Big[\lambda_f \frac{\partial T_f}{\partial z} \Big]_{z_{i-\frac{1}{2}}}^{z_{i+\frac{1}{2}}} + A_{cyl} h (T_{m,i} - T_{f,i}) \\
\rho c_p V_i \frac{\mathrm{d}T_{f,i}}{\mathrm{d}t} &= P_{rod,i} + \frac{\pi D_{rod}^2}{4} \sum_j^{N_i} \lambda_f \frac{T_{f,j} - T_{f,i}}{d_{ij}} + A_{cyl} h (T_{m,i} - T_{f,i})
\end{aligned} \tag{2.20}$$

V_i is the volume of the i^{th} fuel rod element, $T_{f,i}$ is the average temperature of the i^{th} fuel rod element, $P_{rod,i}$ is the total power generated in the i^{th} fuel rod element, D_{rod} is the diameter of the fuel rod, d_{ij} is the distance between the centers of element i and j, N_i is the number of adjacent nodes of node i, A_{cyl} is the area of the cylinder jacket of the fuel rod element, h is the heat transfer coefficient of the fuel pin's surface to the coolant and finally $T_{m,i}$ is the temperature of the moderator fluid. The integration over the middle term on the left hand side is from $z_{i-\frac{1}{2}}$ to $z_{i+\frac{1}{2}}$, because this term concerns the heat exchange between adjacent nodes and happens at the interfaces of the nodes. The heat loss in the upper and

bottom nodes are neglected as they are assumed to be very small compared to the heat loss from the fuel rod through the cylinder wall to the moderator.

However, for the Doppler feedback mechanism in the model only the change of the fuel temperature with respect to the steady state is necessary. Therefore, the steady state solution of Eq. 2.20 is subtracted from the equation and by defining the variables as $x = x_{SS} + x'$ the following equation is left, where the variable x' now represent the variations from the steady state solution.

$$\rho c_p V_i \frac{\mathrm{d}T'_{f,i}}{\mathrm{d}t} = P'_{rod,i} + \frac{\pi D^2_{rod}}{4} \sum_j^{N_i} \lambda_f \frac{T'_{f,j} - T'_{f,i}}{d_{ij}} + A_{cyl} h (T'_{m,i} - T'_{f,i}) \tag{2.21}$$

With this equation the temperature change of each fuel element can be calculated using the variation in power, given by the nodal kinetics, and the variation in temperature of the moderator, given by the thermal hydraulics code. The heat transfer coefficient of the fuel pin's surface to the coolant is given by:

$$h = Nu \frac{\lambda_m}{D_H} \tag{2.22}$$

Nu represents the Nusselt number, D_H is the hydraulic diameter of the fuel rod and λ_m is the heat conductivity of the moderator/coolant. The Nusselt number has proven to be difficult to determine for fluids at supercritical properties and especially around the pseudo critical point properties change significantly. Pioro et al. [25] gave an overview of various correlations found in literature trying to describe heat transfer in tube, annulus and bundle geometries, with the most accurate one, the Krasnoshchekov-Protopopov correlation, predicting 97% of the experimental data for water and carbon dioxide with an accuracy of 25% [13]. However, this correlation was found for tube geometries and not for the bundle geometry in the HPLWR core configuration. Still, in the HPLWR project an altered version of the Krasnoshchekov-Protopopov correlation is proposed to predict the heat transfer, with a side note that more experimental research towards heat transfer in bundle geometries at supercritical conditions is necessary [32]. Unfortunately, to implement this correlation the actual wall temperature is needed and Eq. 2.21 being a rough approximation to calculate the average temperature of the fuel rod it is unnecessary to use an extensive correlation as the one proposed for the HPLWR. For this reason the simpler Dittus-Boelter correlation is used in this research to approximate the heat transfer from the fuel rod to the bulk.

$$Nu = 0.023 Re^{0.8} Pr^n \qquad \text{for } 0.7 \leq Pr \geq 160 \text{ and } Re > 10^4 \tag{2.23}$$

Here n equals 0.4 for heating and 0.3 for cooling. This relation was developed for heat transfer at subcritical pressures, so it will most likely be a rough and simple approximation.

Besides its value for the Doppler feedback, Eq. 2.21 also holds another important purpose. In a nuclear reactor the power generated by the fuel rods can quickly change due to a change in neutron transport. However, the actual heat transfer from the fuel rod to the coolant does not follow this change in power instantaneously. The temperature in the middle of the fuel rod section rises, but it takes a certain time to conduct the heat towards the outer surface, not to mention there is also a fuel cladding in place between the fuel and the coolant. This cladding is however neglected in Eq. 2.21 and only the time delay of the heat transfer in the fuel is taken into account. If this time delay is large, the temperature of the fuel could reach high values, because it cannot dissipate its heat in time, therefore putting stress on the materials. Furthermore, such a delay in heat transfer could also have consequences for the stability of the system. A delayed heat transfer together with the feedback mechanisms can introduce positive feedback in the dynamic transfer function of the system that leads to an unstable state of the reactor.

Chapter 3

Numerical model

This chapter gives an overview of how the SLIMR core has been modeled with *Serpent* [18] and the way the reactivity feedback coefficients are determined. Also the coupling of the thermal hydraulic code for the SLIMR [36] with the nodal kinetics model, as worked out in Section 2.4, is elaborated.

3.1 Serpent model

The nodal kinetics model developed in Section 2.4 requires a steady state neutron density and reactivity feedback coefficients to determine the change in reactivity when perturbations to the steady state of the system are introduced. To this end *Serpent* [18] is used to calculate these values. *Serpent* is a three-dimensional continuous-energy Monte Carlo reactor physics burn-up calculation code. It was firstly developed at VTT Technical Research Centre of Finland in 2004 with spatial homogenization as the main intended application. Since then the code has been improved and more features have been added. For this research *Serpent* is only used for spatial homogenisation of cross sections, the diffusion coefficient and the generation time. *Serpent* uses ACE format data libraries to read continuous-energy cross sections, and for this research the JEFF-3.1 database is used. For 432 nuclides at six temperatures, ranging from 300 K to 1800 K, interaction cross section data is available. Classical collision kinematics, ENDF reaction laws and probability table sampling in the unresolved resonance region are used for the interaction physics. [18]

Serpent requires an input file with all the details of the core configuration, that is; geometry, fuel composition, materials, lattice configuration. Also certain options have to be set for *Serpent* to know which calculations to perform. The input for the SLIMR core configuration is summarised in the next sections.

3.1.1 Fuel assembly

The design of the fuel assemblies of the new SLIMR core has been based on the HPLWR core for reasons discussed in Section 2.2. Figure 2.1(b) gives the configuration of the fuel assembly without a moderator box. The HPLWR fuel assemblies have a moderator box in the middle in which relatively cold water flows to enhance the moderation of the neutrons. For simplicity reasons regarding the thermal-hydraulic code the moderator box has been excluded in the design of the SLIMR core. This will have an effect on the

axial power distribution, because the moderator box is used in the HPLWR design to drive relatively cold water downwards from the top of the core to enhance moderation throughout the core[1]. The fuel pins are surrounded with a cladding made of solid steel (SS 1.4970) and the wall of the fuel assembly box consists of a different type of solid steel (SS 347). In reality the fuel assembly wall is constructed of a SS 347 honeycomb structure filled with ZrO2, but due to the complexity of modeling this in *Serpent* [18] a solid wall of SS 347 is used. Between the fuel pins and the fuel assemblies water is present. Furthermore, the fuel consists of enriched UO_2. The required enrichment to ensure a critical core is explored in Section 4.2.1. Table B.1 presents the measurements of the fuel assembly. [32]

3.1.2 Core configuration

Figure 3.1 illustrates a more detailed lattice configuration than the one introduced in Section 1.2.3. The difference in colors indicate the different temperatures of the water in each heating section, i.e. the Evaporator and Superheater I and II. The whole core is surrounded by a layer of water that has the same temperature as the water in Superheater II. This layer of water acts as a reflector and has a density around 150 kg/m^3. Therefore the reflective layer of water is roughly 20 cm thick to cover the mean free path of neutrons in water. Furthermore, the SLIMR Evaporator holds 57 fuel assemblies and the Superheaters both consists of 64 fuel assemblies. The core has an equivalent diameter of 1.37 m and a height of 4.25 m. In the Appendix the side view of the reactor core is given. The figure has many details, but it gives an idea on how the core is divided into axial and radial nodes. The core is divided into seventeen axial layers with a thickness of 25 cm, which each consist of three radial nodes, i.e. the Evaporator and Superheater I and II. From the inlet of the Evaporator to the outlet of Superheater II the water thus flows through 51 nodes in which the water heats up. *Serpent* [18] requires a density profile of the water, so for each node the density of the water must be known. This density profile comes from the thermal hydraulic model and is on its turn dependent on the power distribution in the core, which comes from *Serpent*. An iteration is thus required and after a few runs of both programs a density profile closer to reality is obtained. This density profile is indicated in Figure A.2(a) with various different colors. The mixing chambers and all other components present in the actual design of the HPLWR are left out due to the complexity of modeling these in *Serpent*. Table B.1 in Appendix B gives an overview of the geometry and configuration of the core. An overview of the input options of *Serpent* are also given Appendix B.

3.2 Reactivity feedback coefficients

The nodal method used to model the neutronics in the core requires a space dependent reactivity, ρ_i. In steady state conditions this reactivity is set to zero by default, because the reactor is assumed to be critical. However, the reactivity changes when perturbations are introduced upon the steady state. The two feedback mechanisms described in section 2.3 are taken into account in this research; Doppler feedback and moderator feedback. Therefore the nodal dependent reactivity is only dependent on the change of the temperature of the fuel, T_f, and the density of the moderator, ρ_m, in the specific node. To calculate the change in the nodal dependent reactivity a linear approximation with respect to the before mentioned parameters is used, which will be explained further ahead. For this linear relationship reactivity feedback coefficients, α_f and α_ρ need to be determined. These coefficients are defined as follows.

$$\alpha_{T,i} = \frac{\partial \rho_i}{\partial T_{f,i}} \text{ and } \alpha_{\rho,i} = \frac{\partial \rho_i}{\partial \rho_{m,i}} \tag{3.1}$$

[1] Especially at the top of the core, where the average density of the moderator is smaller than in the bottom, moderation is enhanced.

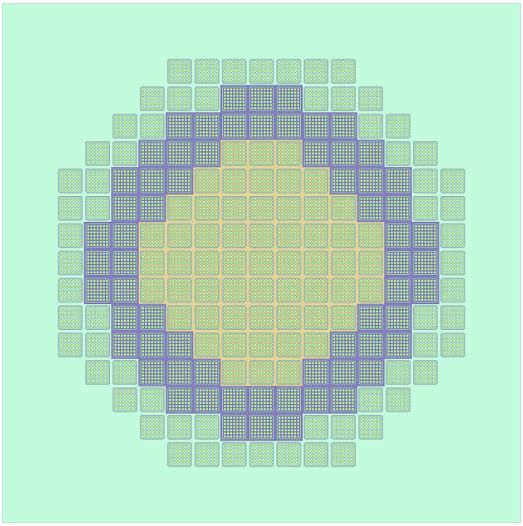

Figure 3.1: SLIMR core configuration. The difference in colors indicate the different temperature of the water in each heating section, i.e. the Evaporator and Superheater I and II

Serpent can be used to this end. To determine the reactivity feedback coefficients different core setups are given as input to *Serpent*, i.e. the density and fuel temperature is varied in each node. The reactivity is defined as follows;

$$\rho_i = \frac{k_i - 1}{k_i} \tag{3.2}$$

And for calculating the multiplication factor k the following relation is used:

$$k_i = \frac{\nu\Sigma_{f,i}}{\Sigma_{a,i}} \tag{3.3}$$

These node dependent fission and absorption cross sections are calculated through homogenisation in space and energy. This approximation should yield a result that is comparable with the result when it would have been calculated with all the details in the spatial and energy domain. Due to the nodal kinetics method in this research, the cross sections need to be homogenised for each node to get nodal dependent multiplication factors and therefore reactivity for each node. To calculate the average cross sections for each node, the following relation is used.

$$\bar{\Sigma}_{x,i} = \frac{\int_{V_i}\int_E \Sigma_{x,i}(\mathbf{r},E)\phi(\mathbf{r},E)\mathrm{d}^3\mathbf{r}\mathrm{d}E}{\int_{V_i}\int_E \phi(\mathbf{r},E)\mathrm{d}^3\mathbf{r}\mathrm{d}E} \tag{3.4}$$

Where $\bar{\Sigma}_{x,i}$ is the macroscopic cross section averaged over a node. The integrals over the fission rate, absorption rate and the neutron flux density itself can be performed with the use of detectors in each node of the core, a function incorporated in *Serpent* [18]. As changes in the multiplication factor due to changes in moderator density and fuel temperature are rather small, for example in the order of $\sim$1% for a density increase of 200 kg/m^3, the calculations need to be precise on a level of 10 pcm to get consistent feedback reactivity coefficients. This means that for a Monte Carlo based code as *Serpent* the calculations

need to run with a large neutron population and numerous active cycles, this unfortunately increases the computational time. This large computational time is the reason for using a linear approximation, because depending on the desired accuracy the calculation for one node can take up to 90 hours. So therefore, a change in temperature of the fuel and a change in the density of the moderator is introduced only once, and the change in the reactivity of that specific node is then calculated using k_i from the steady state calculation. The density in a specific node is increased with 0.2 g/cm^3 and the fuel temperature is increased with 300 K. This rather large increase is chosen to make sure the inaccuracy of the calculations is not too large compared to the actual change in reactivity. Section 4.2.3 will examine if this linear approximation is valid. Finally, in the model the nodal reactivity can be calculated using the following relationship:

$$\rho_i = \alpha_{T,i}\Delta T_{f,i} + \alpha_{\rho,i}\Delta\rho_{m,i} \tag{3.5}$$

Where $\Delta T_{f,i}$ and $\Delta\rho_{m,i}$ represent the change with respect to the steady state of the fuel temperature and moderator density respectively in each node.

3.3 Thermal hydraulics and nodal kinetics

3.3.1 Previous work

The feasibility study by Veling [36] was performed with the one-dimensional thermal hydraulics model, the SLIMR model. This model can perform transient calculations on the thermal hydraulic stability of the natural circulation flow in the RPV of the SLIMR, the heat transfer from the inner RPV wall to the outer RPV wall and the heat balance of the pool in which the RPV is submerged. However, in this research the focus lies only at the natural circulation flow inside the RPV, which makes the model that performs calculations on the heat transfer to the RPV wall and the pool irrelevant for the purpose of this research. Therefore, only the one-dimensional loop model for the natural circulation flow inside the RPV is described here. The SLIMR model is based on the DeLight code, which was developed to simulate the natural circulation flow of supercritical Freon R23 in the DeLight facility. Due to the hardcoded geometry of the DeLight setup and the ability to only simulate forward flows, the DeLight code was not a fit for the transient calculations for the SLIMR design and the SLIMR model was developed. The SLIMR model can handle both forward and backward flows (especially important for SCRAM scenarios), can be used for multiple geometries and is written in *Matlab*. [36]

Spacial discretization

To perform the transient calculations on the flow the conservation equations have been discretized in both space and time. The Finite Volume Method (FVM) is used to discretize in space and towards this end the SLIMR is divided into a finite number of non-overlapping cells, making sure the conservation equations hold. Two steps are involved when using the FVM, first the equations are integrated over the control volume and then the integrated equations are being discretized [36]. This method is already being demonstrated in Section 2.4, where the point kinetics equations are integrated over the volume of each node and discretized in space. There is however a difference in the type of grid used between the nodal kinetics model and the flow model in the SLIMR model. The SLIMR model uses a staggered grid, meaning that the control volume is not the same for every conservation equation. Two grids are used in the flow model, one to store the cell-averaged value of the pressure and fluid properties in the center of the main control volume and thus used in the mass and energy conservation equations. The other is used to store velocity components on the faces of the main control volume, thus used for the conservation of

momentum equation. The nodal kinetics model uses an unstaggered grid and properties are stored in the middle of the control volume.

Temporal discretization

Discretization in time is done by Veling [36] with the semi-implicit Euler method. This method is a combination of the forward and backward Euler methods, which are used to solve ordinary differential equations, i.e. $\frac{\mathrm{d}y}{\mathrm{d}t} = f(t, y)$. The forward[2] Euler method solves the next time step with the following equation:

$$y^{n+1} = y^n + f(t_n, y^n)\Delta t \tag{3.6}$$

The advantage of this method is its computational speed, but the method is not unconditionally stable and must therefore meet two criteria to ensure numerical stability. In contrast with this, the backward[3] Euler method is unconditionally stable, but requires more computational time. The next time step is then calculated as follows:

$$y^{n+1} = y^n + f(t_{n+1}, y^{n+1})\Delta t \tag{3.7}$$

The semi-implicit Euler method is a combination of both methods and to what extend each method is used is determined with θ, see Eq. 3.8. When $\theta = 1$ the ordinary differential equations will be solved with the backward Euler method and when $\theta = 0$ the forward method is used. Any value between 0 and 1 will combine both methods, with $\frac{1}{2}$ representing the Crank-Nicolson method. The semi-implicit Euler method is used by Veling [36] in the flow model and will also be used for the nodal kinetics equations and the fuel temperature equation to ensure a coherent code.

$$y^{n+1} = y^n + \theta f(t_{n+1}, y^{n+1})\Delta t + (1-\theta) f(t_n, y^n)\Delta t \tag{3.8}$$

Flow chart of the original SLIMR model

To understand how the coupling of the nodal kinetics model and the thermal hydraulics model is integrated in the SLIMR model, the flow chart of the SLIMR algorithm as given by Veling [36] is presented in Figure 3.2 in white and explained. The steps indicated with red are the addition of this work and are explained in the next section. This flowchart excludes the heat transfer in the RPV wall and the pool energy balance as it lies out of the scope of this research. In the first eight steps the necessary information is given in order to perform the calculations, this includes the input of data for the spline functions[4], determining simulation details and geometry parameters, allocation of variables, setup of the grid and indices and lastly the initial conditions are set. After the setup the model starts with the time stepping loop and the power is first defined with an S-shaped function. The power starts at zero and increases till the required power in the specified time, after which the model runs for another specified amount of time to reach a steady state flow inside the reactor. After the core power is defined the properties of the coolant flow, e.g. the mass flow rate and enthalpy, are calculated for the next time step using the flow model. In the flow model the discretized conservation equations, such as the enthalpy and the momentum balance, together with splines are used to calculate these properties. After the flow model is done the model goes back to defining the core power until the specified time is reached. Data is saved for later analysis. For a more detailed explanation of the working of the thermal hydraulics code of Veling I refer to his thesis [36].

[2] The forward Euler method is also known as the explicit Euler method.
[3] The backward Euler method is also known as the implicit Euler method.
[4] Spline functions are used to approximate and calculate the properties of water at a pressure of 25 MPa.

3.3.2 SLIMR model with neutronic feedback

The inclusion of the coupling of the neutronics and the thermal hydraulics has been done by complementing the SLIMR code with two models; the nodal kinetics and the fuel temperature model. Figure 3.2 shows the addition (in red) to the SLIMR model. The power of the reactor still increases with an S-shaped function in the start-up phase, but after this phase the core power is defined using the neutron density calculated by the nodal kinetics model. Based on the temperature of the fuel, the density of the coolant and the previous neutron density profile the new neutron density profile is calculated. The power changes proportional to the changes in the neutron density and is thus updated in every time step according to the changes in the temperature of the fuel and the density of the moderator. In order to implement the effect that the Doppler feedback and the moderator density feedback have on the core power, reactivity feedback coefficients α_ρ and α_T are loaded. Separately from the SLIMR model core calculations with *Serpent* (in cyan) are performed before the SLIMR model is started. These calculations are only done once, before the SLIMR model is started, and give the reactivity feedback coefficients and steady state neutron density, n_{SS} for every node in the core. Furthermore, *Serpent* calculates the generation time, neutron speed and the diffusion coefficient for the core, necessary for the nodal kinetics model. Finally, after the flow model has calculated the properties of the flow, the fuel temperature model calculates the new fuel temperature inside the core[5].

The original model as used by Veling [36] has been held as a benchmark to test the new model including neutronics. The new model does incorporate a three-pass core, but by implementing the original core design of Veling [36] the new model could be benchmarked. For steady state conditions the models showed similar results.

[5] In practice the deviation in fuel temperature is calculated as the reactivity in the steady state is defined to be zero and the deviation in fuel temperature will suffice.

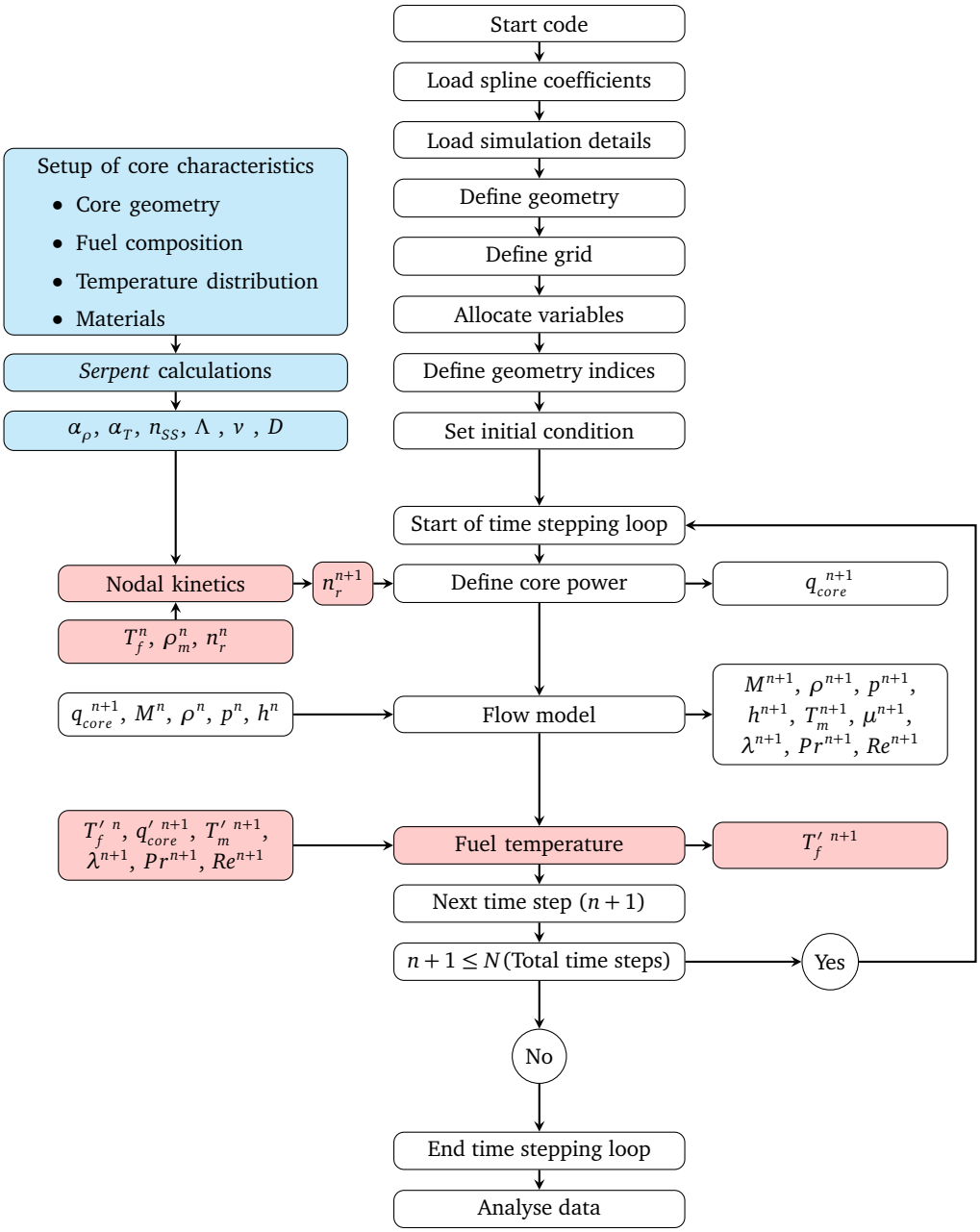

Figure 3.2: The SLIMR algorithm with coupling between the neutronics and thermal hydraulics. The boxes indicated in red are added in this research to the algorithm of Veling [36]. The boxes in cyan represent the steps taken with *Serpent*, which are taken before the SLIMR model begins. The indices i indicating nodes of the variables are left out for clarity of the diagram.

Temporal discretization of the nodal kinetics equations

In Section 2.4 the spatial discretization has already been explained, as it is a main aspect of the nodal kinetics model. This part will cover the temporal discretization of the nodal kinetics equations and therefore begins with integrating Eq. 2.15. The same method for temporal discretization as used by Veling [36] is being applied here to make the model as a whole coherent.

$$\begin{cases} \displaystyle\int_{t^n}^{t^{n+1}} \frac{\mathrm{d}n_{r,i}(t)}{\mathrm{d}t}\mathrm{d}t = \int_{t^n}^{t^{n+1}} \frac{\rho_i-\beta-\xi_{i,i}}{\Lambda_i} n_{r,i}(t)\mathrm{d}t + \int_{t^n}^{t^{n+1}} \frac{1}{\Lambda_i}\sum_{j=1}^{N_i}\xi_{i,j}n_{r,j}(t)\mathrm{d}t + \int_{t^n}^{t^{n+1}} \sum_{k=1}^{6}\lambda_k C_{r,k,i}(t)\mathrm{d}t \\ \displaystyle\int_{t^n}^{t^{n+1}} \frac{\mathrm{d}C_{r,k,i}(t)}{\mathrm{d}t}\mathrm{d}t = \int_{t^n}^{t^{n+1}} \lambda_k\big(n_{r,i}(t)-C_{r,k,i}(t)\big)\mathrm{d}t \quad \text{with } k=1\ldots6 \end{cases} \tag{3.9}$$

Remind, $\xi_{i,i}$ and $\xi_{i,j}$ are coupling coefficients defined in Eq. 2.16 and Eq. 2.17. Every term in the nodal kinetics equations has to be worked out and to do that an intermediate time step has to be defined. To integrate the time dependent variables on the right hand side of the equations the following time step (Eq. 3.10) is introduced in order to implement the semi-implicit Euler method discussed in Section 3.3.1. Also Eq. 3.11 gives an example of the approximation that is made when integrating over a variable.

$$t_n + \theta\Delta t_n := t_{n+\theta} \tag{3.10}$$

$$\int_{t^n}^{t^{n+1}} x(t)\mathrm{d}t \approx x(t_{n+\theta})\Delta t_n \tag{3.11}$$

Using these definitions another definition is introduced to simplify the notation of variables and comply with the semi-implicit Euler method, that is:

$$x(t_{n+\theta}) = x^{n+\theta} := \theta x^{n+1} + (1-\theta)x^n \tag{3.12}$$

From this point on working out the equations is straight forward.

$$\begin{cases} \big[n_{r,i}(t)\big]_{t_n}^{t_{n+1}} = \dfrac{\rho_i-\beta-\xi_{i,i}}{\Lambda_i} n_{r,i}^{n+\theta}\Delta t_n + \dfrac{1}{\Lambda_i}\displaystyle\sum_{j=1}^{N_i}\xi_{i,j}n_{r,j}^{n+\theta}\Delta t_n + \sum_{k=1}^{6}\lambda_k C_{r,k,i}^{n+\theta}\Delta t_n \\ \big[C_{r,k,i}(t)\big]_{t_n}^{t_{n+1}} = \lambda_k\big(n_{r,i}^{n+\theta} - C_{r,k,i}^{n+\theta}\big)\Delta t_n \quad \text{with } k=1\ldots6 \end{cases} \tag{3.13}$$

Now by using Eq. 3.12 in working out the left hand side of the equations Eq. 3.13 is obtained. The variables that need to be calculated are given in blue.

$$\begin{cases} n_{r,i}^{n+1} - n_{r,i}^{n} = \left(\theta \dfrac{\rho_i - \beta - \xi_{i,i}}{\Lambda_i} n_{r,i}^{n+1} + (1-\theta)\dfrac{\rho_i - \beta - \xi_{i,i}}{\Lambda_i} n_{r,i}^{n}\right)\Delta t_n \\ \qquad\qquad + \dfrac{1}{\Lambda_i}\displaystyle\sum_{j=1}^{N_i} \xi_{i,j}\left(\theta n_{r,j}^{n+1} + (1-\theta) n_{r,j}^{n}\right)\Delta t_n \\ \qquad\qquad + \displaystyle\sum_{k=1}^{6} \lambda_k \left(\theta C_{r,k,i}^{n+1} + (1-\theta) C_{r,k,i}^{n}\right)\Delta t_n \\ C_{r,k,i}^{n+1} - C_{r,k,i}^{n} = \lambda_k\left(\theta(n_{r,i}^{n+1} - C_{r,k,i}^{n+1}) + (1-\theta)(n_{r,i}^{n} - C_{r,k,i}^{n})\right)\Delta t_n \quad \text{with } k = 1\ldots 6 \end{cases} \tag{3.14}$$

These seven equations[6] are setup for every node of the core. So in total there will be seven times the number of nodes of equations and variables to be solved. How this system of linear equations is solved is explained in Section 3.3.3.

Temporal discretization of the fuel temperature

The temporal discretization of the fuel temperature equation (Eq. 2.21) is similar to the previous discretization and begins with Eq. 3.15.

$$\rho c_p V_i \int_{t^n}^{t^{n+1}} \frac{\mathrm{d}T'_{f,i}(t)}{\mathrm{d}t}\mathrm{d}t = \int_{t^n}^{t^{n+1}} P'_{rod,i}(t)\mathrm{d}t + \frac{\pi D_{rod}^2}{4}\int_{t^n}^{t^{n+1}} \sum_{j}^{N_i} \lambda_f \frac{T'_{f,j}(t) - T'_{f,i}(t)}{d_{ij}}\mathrm{d}t + A_{cyl} h \int_{t^n}^{t^{n+1}} (T'_{m,i}(t) - T'_{f,i}(t))\mathrm{d}t \tag{3.15}$$

Remind, as defined in Section 2.5 N_i is the number of adjacent nodes of fuel rod element i. Applying Eq. 3.12 and 3.11 and skipping ahead to the final form gives Eq. 3.16 and again the unknown variables that are needed for the next time step are indicated in blue. Notice that the other variables, i.e. $P'_{rod,i}$ and $T'_{m,i}$, have already been calculated with the nodal kinetics and the flow model respectively.

$$\begin{aligned} \rho c_p V_i (T'^{\,n+1}_{f,i} - T'^{\,n}_{f,i}) = &\left(\theta P'^{\,n+1}_{rod,i} + (1-\theta) P'^{\,n}_{rod,i}\right)\Delta t_n \\ &+ \frac{\pi D_{rod}^2}{4}\sum_{j}^{N_i} \frac{\lambda_f}{d_{ij}}\left(\theta(T'^{\,n+1}_{f,j} - T'^{\,n+1}_{f,i}) + (1-\theta)(T'^{\,n}_{f,j} - T'^{\,n}_{f,i})\right)\Delta t_n \\ &+ A_{cyl} h\left(\theta(T'^{\,n+1}_{m,i} - T'^{\,n+1}_{f,i}) + (1-\theta)(T'^{\,n}_{m,i} - T'^{\,n}_{f,i})\right)\Delta t_n \end{aligned} \tag{3.16}$$

In total there will be the same amount of equations as there are nodes in the core. How this system of linear equations is solved is explained next.

3.3.3 Solving the linear system of equations

The system of linear equations derived in Section 3.3.2 lacks a convenient structure due to the six precursor equations and the exchange of neutrons between the Evaporator and the Superheaters. For this

[6] One equation for the neutron density and six equations for the six precursor groups.

reason the `linsolve` function of *Matlab* is used to solve the system. This function is based on LU decomposition and takes more computational power than the algorithm that is explained next. For the fuel temperature model a more suitable algorithm can be used to solve the system of linear equations. Koopman [16] described this algorithm and it has already been used in the SLIMR model of Veling [36]. In matrix form the system of linear equations can be written as:

$$\underline{\underline{A}} \cdot \underline{\phi} = \underline{s} \tag{3.17}$$

Where $\underline{\phi}$ holds all the unknown variables, in this case the fuel temperature of the next step $n+1$ for all nodes. $\underline{\underline{A}}$ carries all the terms dependent on $\underline{\phi}$ and $\underline{s}$ carries all the independent terms. The first order upwind scheme used to discretize the energy balance of the fuel temperature model[7] makes $\underline{\underline{A}}$ a tri-diagonal matrix, which makes Eq. 3.17 of the form:

$$\begin{bmatrix} b_1 & c_1 & 0 & \dots & \dots & 0 \\ a_2 & b_2 & c_2 & & & \vdots \\ 0 & \ddots & \ddots & \ddots & & \vdots \\ \vdots & & \ddots & \ddots & \ddots & 0 \\ \vdots & & & a_{N-1} & b_{N-1} & c_{N-1} \\ 0 & \dots & \dots & 0 & a_N & b_N \end{bmatrix} \cdot \begin{bmatrix} \phi_1 \\ \phi_2 \\ \vdots \\ \vdots \\ \phi_{N-1} \\ \phi_N \end{bmatrix} = \begin{bmatrix} s_1 \\ s_2 \\ \vdots \\ \vdots \\ s_{N-1} \\ s_N \end{bmatrix} \tag{3.18}$$

For these kind of tri-diagonal systems Koopman [16] used an algorithm which is presented here. This algorithm reduces the computational time of solving the system and is therefore included in the SLIMR model. First, the following parameters are defined:

$$w_1 = b_1, \quad v_1 = \frac{c_1}{w_1} \quad \text{and} \quad z_1 = \frac{s_1}{w_1}$$

Then the other parameters are defined by means of iteration:

$$\begin{aligned} \text{For} \quad i &= 2,3,\dots,N \\ w_i &= b_i - a_i v_{i-1} \\ v_i &= \frac{c_i}{w_i} \\ z_i &= \frac{s_i - a_i z_{i-1}}{w_i} \end{aligned}$$

Where N is the size of the vector $\underline{s}$ and thus equals the number of nodes in each annular node of the core. This means that this equation is solved separately for the Evaporator, Superheater I and Superheater II, because the fuel rod elements only exchange heat axially and not radially towards other fuel rod elements[8]. With these parameters $\underline{\phi}$, containing the unknown variables, can now be calculated with the following relations.

$$\begin{aligned} \phi_N &= z_N \\ \text{For} \quad i &= N-1, N-2, \dots, 1 \\ \phi_i &= z_i - v_i \phi_{i+1} \end{aligned}$$

For proof of this method I refer to Koopman [16].

[7] Only neighbouring nodes exchange heat.

[8] Though the fuel rods do exchange heat radially, but this is absorbed by the coolant.

Chapter 4

Results

4.1 Determining an optimal steady state

Determining the geometry for an optimal and safe design of the SLIMR requires insight in the working and behaviour of the reactor and this insight can be found through a new parameter study. Although Veling [36] already performed an extensive parameter study on the SLIMR, the core configuration and power profile in the core have changed and affect the results. Depending on the conditions and considerations made for the performance and safety of the reactor different set of optimal parameters can be found. Trade-offs between conditions will most certainly have to be made as several conditions conflict with each other. Using the term 'optimal' can become tricky and it is important to explain clearly what is meant with optimal. In this case 'optimal' means that the design parameters of the SLIMR meet the following conditions as best as possible.

Conditions

First of all, the core outlet temperature of the reactor is preferable in the range of 400 °C to 500 °C. One of the reasons to use supercritical water as a coolant is that higher temperatures can be reached, hence a higher efficiency. Though, above 500 °C corrosion of materials start to play a dominant role and damages the integrity of the reactor in the long term. Also surpassing the pseudo-critical temperature is crucial to exploit the benefits of the density drop and the peak in the specific heat capacity.

Secondly, there is the preference for a high thermal power to increase the return on investment of the plant. The size of the SLIMR core and the volume of the fuel are scaled, with respect to the HPLWR, such that a maximum power of 350 MWth can be reached. Increasing the power has implications on the natural circulation flow inside the reactor and careful consideration must be given to the stability of the flow. To this end, mass flow rate (M) vs power (P) curves have been analysed to find stable flows and therefore safe operational points.

Thirdly, a small riser decreases the total size of the RPV and makes handling of the RPV during transport and construction easier, but there are other issues to consider. First, a high riser increases the gravitational pressure drop between the riser and the downcomer and therefore increases the mass flow rate. This has an impact on the outlet temperature and the stability of the flow. Also, a high riser increases the total area of the RPV and thus enhances the heat transfer between the RPV and the surrounding pool during

operational conditions (undesired heat loss), but also during accident scenarios when the decay heat must be removed passively (desired heat loss). In addition, a high riser increases the heat sink during accident scenarios, preventing excessive temperatures inside the RPV. So regarding the height of the riser multiple conditions and constraints have to be considered and will ultimately lead to a trade-off.

Variation of parameters

Adhering to these conditions requires the investigation of more parameters besides the power and riser length. Regarding the previous parameter study of the SLIMR, Veling [36] has investigated the influence of various parameters on the performance of the reactor, i.e. the riser length, riser diameter, inlet temperature, power, core height, downcomer diameter, and core inlet friction. The parameters with the largest effect on the operation of the reactor were found to be the power, riser length, core height and inlet friction. Therefore these parameters will be investigated in the upcoming parameter study, excluding however the core height and including the inlet temperature. The core height will be set equal to 4.25 m[1] to stay close to the geometry of the HPLWR core. The influence of the inlet temperature is also investigated, because it determines the outlet temperature and the size of the density drop. From this parameter study a set of parameters are chosen such that the operation of the SLIMR is optimal and safe, taking into account the conditions just mentioned. These parameters will be used in Section 4.3 to investigate the stability of the design. Table 4.1 gives an overview of the varied parameters.

Table 4.1: The varied parameters.

Parameter	**Range**	**Step**
K_{inlet}	0 - 30	30
L_R	2 m - 10 m	0.25 m
T_{in}	280 °C - 350 °C	5 °C
P	100 MW - 350 MW	25 MW

4.1.1 Simulation procedure

Besides the different core geometry and the use of a more realistic power distribution no further changes were made to the thermal hydraulics code of Veling [36] for this parameter study.[2] For this reason the simulation procedure to let the system reach it steady state is similar to the one in Veling's work [36] and is briefly described here. Reaching steady steady involves two steps:

1 Reaching nominal operating power

2 Damping of mass flow rate oscillations

The first step comprises of increasing the total power of the reactor from zero to the nominal operating power via a S-shaped heating curve. The fluid throughout the entire reactor starts with an equal temperature (the core inlet temperature) and a zero mass flow rate. The duration of this step is 1000 s with a time step of 0.05 s. By increasing the power this way the steady state is reached gradually and mass flow oscillations are prevented. The second step involves simulating the reactor for another 1000 s at the nominal operating power. If the system is not settled after the first step, this second step ensures that

[1] The core height of the HPLWR is 4.2 m, but 4.25 m is more convenient because the grid size in the model is 0.25 m.

[2] The nodal kinetics model and the fuel temperature model are left out, as these are only important for studying the stability of the system.

all the physical quantities of the steady state working point are settled. Finally, when the simulation is finished, the mass flow rate and the core outlet temperature are determined. The fixed parameters and simulations characteristics are giving in table 4.2.

Table 4.2: The fixed geometry parameters of the SLIMR during the parameter study.

SLIMR Dimensions			
Core	Height	4.25	m
	Equiv. Diameter	1.37	m
	Fuel Pin Diameter	8	mm
Riser	Diameter	0.94	m
Heat Exchanger	Length	2.50	m
Downcomer	Outer Annulus Diameter	2.44	m
RPV	Vessel Thickness	0.37	m
Operating Point			
System	Pressure	25	MPa
Simulation Characteristics			
Time	Reaching Nominal Power	1000	s
	Damping Mass Flow Oscillations	1000	s
	Time Step	0.05	s
Semi Implicit Scheme	Theta	1	-
Space	Grid Size	0.25	

From these steady state results a SLIMR geometry will be chosen to investigate the stability of the system. Veling's geometry and input parameters will be used as a basis to explore the influence of the parameters for easy comparison between the results from Veling [36]. This means a power of 150 MW, a riser length of 9 m and an inlet temperature of 280 °C will be used as the fixed parameter to show the results. In the following subsections the line of argumentation is complemented by summarising flow diagrams to increase clarity.

4.1.2 Variation of the core inlet friction

Performing a parameter study with four different parameters (being K_{inlet}, L_R, T_{in} and P) and exploring all the different combinations can become an extensive exercise. Therefore decisions have to be made regarding which parameters to explore extensively and which ones to explore less. The core inlet friction is in this case decided to be one of the less explored parameters, that is; the core inlet friction is either set to 0 or 30. After analysing the influence of the core inlet friction on the performance of the reactor a value is chosen to continue with in the next analyses of the results. Veling [36] stated that the natural circulation BWR has a typical core inlet friction of 30 and he assumes this value could be applied to the SLIMR as well.

Figure 4.1 shows the results for two cases; Figure 4.1(a) and 4.1(b) show the mass flow rate and the core outlet temperature for the case in which $K_{\text{inlet}} = 0$ (and L_R=9 m), and for the bottom two graphs the core inlet friction is equal to 30. What can be seen from the graphs is that the core inlet friction has a significant influence on the mass flow rate of the natural circulation. Additional friction in the water loop adds resistance to the flow and lowers the mass flow rate. Subsequently, a lower mass flow rate at a

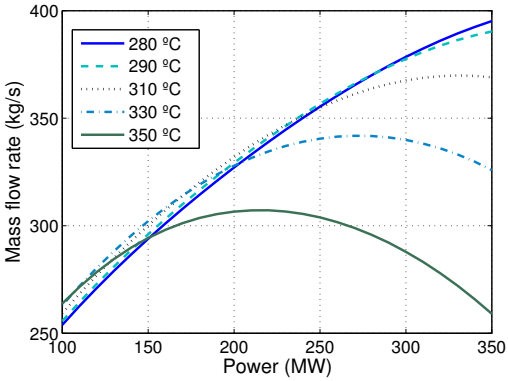

(a) Mass flow rate for a reactor with $L_R = 9m$ and $K_{\text{inlet}} = 0$ for a range of inlet temperatures.

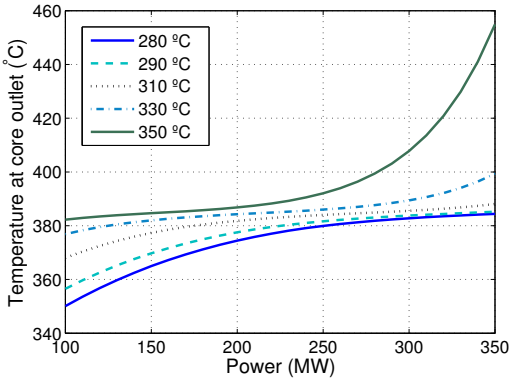

(b) Core outlet temperature for a reactor with $L_R = 9m$ and $K_{\text{inlet}} = 0$ for a range of inlet temperatures.

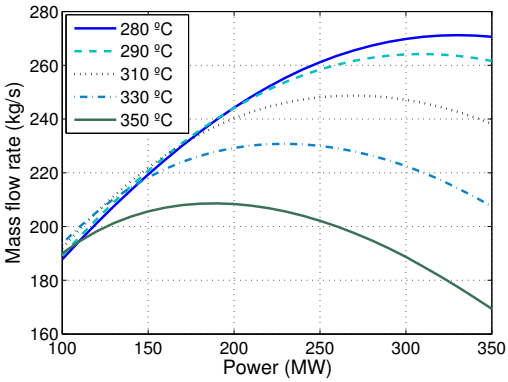

(c) Mass flow rate for a reactor with $L_R = 9m$ and $K_{\text{inlet}} = 30$ for a range of inlet temperatures.

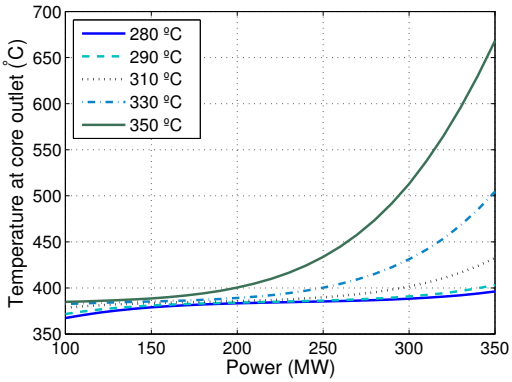

(d) Core outlet temperature for a reactor with $L_R = 9m$ and $K_{\text{inlet}} = 0$ for a range of inlet temperatures.

Figure 4.1: Varying the power to see the influence on the mass flow rate and core outlet temperature for $K_{\text{inlet}} = 0$ and $K_{\text{inlet}} = 30$, at various inlet temperatures.

specific power causes the core outlet temperature to increase as more heat is supplied to less mass, thus beneficial for the efficiency of the reactor.

$$K_{\text{inlet}} \Uparrow \longrightarrow \text{Resistance} \Uparrow \longrightarrow M \Downarrow \longrightarrow T_{\text{out}} \Uparrow$$

Figure 4.1(a) and 4.1(b) show that at $K_{\text{inlet}} = 0$ the mass flow rate is too high to reach a desired core outlet temperature. Only for a high inlet temperature (e.g. 350 °C) and a high power (e.g. 350 MW) the core outlet temperature becomes sufficient, so the choice is made here to set the core inlet friction to 30 to increase the core outlet temperature for a range of other parameters. Decreasing the riser length is also an option to lower the mass flow rate, but for reasons explained in the next section the riser is preferred to be high.

4.1.3 Variation of the riser length

Information on the behaviour of the reactor in steady state upon changing the riser length has been obtained by running the SLIMR model with various riser lengths, ranging from 2.00 to 10.00 m in steps of 0.25 m for different values of the power and inlet temperature. Figure 4.2 shows two graphs in which the influence of the riser length on the mass flow rate and the core outlet temperature can be seen for a power of 150 MW. Next, the influence of the riser length on the core outlet temperature for different inlet temperatures is analysed and M vs P curves are being examined to decide on an optimal range of riser lengths.

As expected the mass flow rate increases with larger riser lengths (Figure 4.2(a)) which causes a decrease in core outlet temperature.

$$L_R \Uparrow \quad \longrightarrow \quad \Delta p_{\text{gravitation}} \Uparrow \quad \longrightarrow \quad M \Uparrow \quad \longrightarrow \quad T_{\text{out}} \Downarrow$$

Evidence of the sharp peak in the specific heat capacity of water, as displayed in Figure 1.5, can be found in Figure 4.2(b). For an inlet temperature of 310 °C the mass flow rate steadily decreases for lower riser lengths, but the core outlet temperature does not seem to increase as much. This is due to the large peak in the specific heat, which causes the water to absorb heat without increasing its temperature that much around the pseudo-critical point. After reaching the pseudo critical point the temperature increases faster as more heat is absorbed and this can clearly be seen from the $T_{\text{in}} = 350\,°\text{C}$ graph in Figure 4.2(b). Thus when the reactor operates with a T_{out} just below the pseudo-critical point the riser length does not have much influence on the outlet temperature due to the large peak in specific heat.

Choosing a riser length based on the previous analysis would exclude one important criterion, as it also important where the steady state point lies on the M vs P curve. Figure 4.2(c) shows such curves for a system with an inlet temperature of 280 °C. What can be seen is that these curves have a maximum and after that maximum the power increases while the mass flow rate decreases[3]. This causes a steep increase in outlet temperature as more heat is absorbed by a flow with a lower mass flow rate, see Figure 4.2(d). In general these situations must be avoided, because a more resilient flow is preferable for safety and stability reasons. An ideal operational point would lie around the maximum of the M vs P curve, thus where $\frac{\mathrm{d}M}{\mathrm{d}P} \approx 0$.

Let us consider an example by using Figure 4.2(c) and 4.2(d): If a SLIMR with a riser length of 2 m would operate at 200 MW and suddenly, due to external perturbations, the power would increase to 225 MW the mass flow rate would decrease and cause a core outlet temperature rise of 5.1 °C. In contrast, if the reactor would operate at 250 MW and the power would increase to 275 MW, the temperature would increase 23.8 °C. Hence, this temperature increase becomes bigger when the operational point lies more to the right of the maximum in the M vs P curve. Therefore, ideally the operational point should lie around the maximum of the M vs P curve to ensure a stable system. Any perturbations in the power, either a decrease or increase, has less effect on the mass flow rate and thus on the core outlet temperature. In this example a power of 200 MW would be better.

Keeping this in mind and considering the five curves shown in Figure 4.2(c) a larger riser length is preferable as the maximum of the curve shifts to the right, enabling the reactor to operate at a higher power in a stable state. The $\frac{\mathrm{d}M}{\mathrm{d}P} = 0$ point of the M vs P curve lies to the right of 300 MW for riser lengths above 8 m. Also, a higher riser would be beneficial for the safety of the reactor. Not only does the RPV has more surface to exchange heat with the pool, the RPV also contains more water in general.

[3] The mass flow rate decreases for higher powers because the frictional pressure drop increases faster than the gravitational pressure drop due to a large density drop resulting in a high fluid velocity.

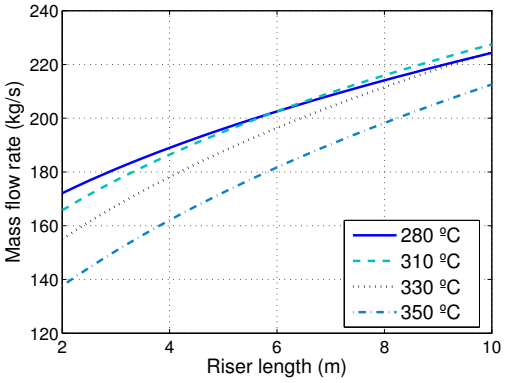

(a) Mass flow rate for a reactor with P=150 MW and various inlet temperatures.

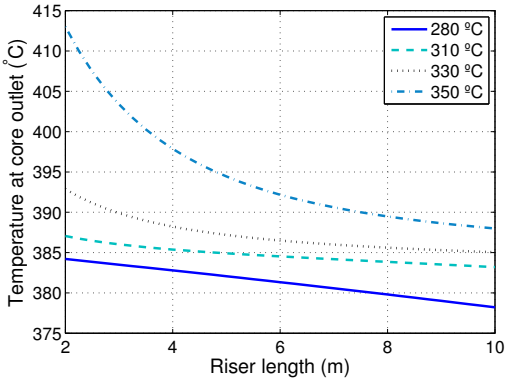

(b) Core outlet temperature for a reactor with P=150 MW and various inlet temperatures.

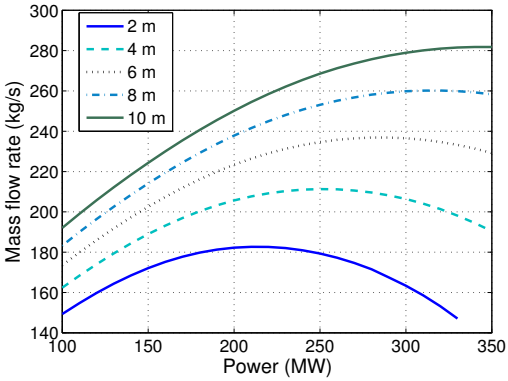

(c) Mass flow rate for a reactor with T_{in}=280 °C and various riser lengths.

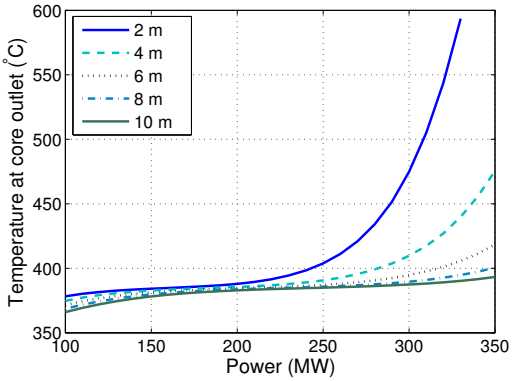

(d) Core outlet temperature for a reactor with T_{in}=280 °C and various riser lengths.

Figure 4.2: Varying the power and the riser length to see the influence on the mass flow rate and core outlet temperature.

This enlarges the heat sink during accident scenarios when the decay heat heats up the water inside the RPV and heat is only transferred away through the RPV wall to the pool.

However, a too large riser length impedes the ability to go to the desired core outlet temperature (400 °C-500 °C), see Figure 4.2(d). So for these reasons the desired range of the riser length will be between 8 m and 10 m.

4.1.4 Variation of the inlet temperature

The inlet temperature is varied from 280 °C to 350 °C in steps of 5 °C. Too low inlet temperatures will prevent the reactor from surpassing the pseudo-critical point and affect the efficiency of the reactor, and too high inlet temperatures (in the annular downcomer) lead to high thermal losses with the surroundings during nominal operation [36]. The mass flow rate remains constant for lower inlet temperatures and

decreases when inlet temperature becomes higher, see Figure 4.3.

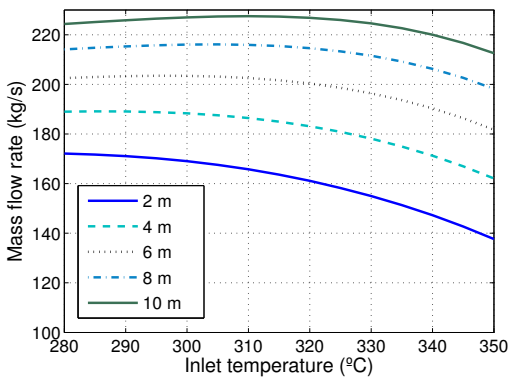

(a) Mass flow rate for a reactor with P=150 MW and various riser lengths.

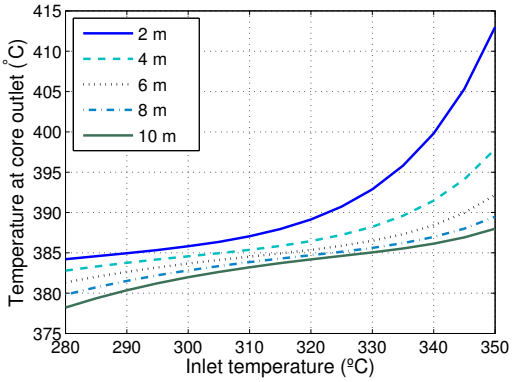

(b) Core outlet temperature for a reactor with P=150 MW and various riser lengths.

Figure 4.3: Varying the inlet temperature to see the influence on the mass flow rate and core outlet temperature.

The results in Figure 4.3(a) can be explained with the density drop over the core and the velocity of the fluid (Figure 4.4). The density difference over the core increases when the inlet temperature approaches the strong density drop near the pseudo-critical point, see Figure 1.5. The large density difference increases the gravitational pressure difference between the riser and the downcomer. At the same time the fluid expands more and the velocity of the fluid increases at the core outlet, see Figure 4.4(b). Due to the higher velocity the frictional pressure drop over the loop increases because the wall shear stress, $\tau_{w\rightarrow f}$, is proportional to the square of the velocity of the fluid [36]. The frictional pressure drop over the loop increases faster than the gravitational pressure drop and the mass flow rate decreases. Lower mass flow rates at a constant power result in lower outlet temperatures.

$$T_{\text{in}} \Uparrow \longrightarrow \Delta\rho_m \Uparrow \longrightarrow v_{\text{outlet}} \Uparrow \longrightarrow \Delta p_{\text{friction}} \Uparrow > \Delta p_{\text{gravitation}} \Uparrow \longrightarrow M \Downarrow \longrightarrow T_{\text{out}} \Uparrow$$

Reconsidering Figures 4.1(c) and 4.1(d), it can be seen that the maxima of the M vs P curves shift towards the right and upwards for decreasing inlet temperatures. The same argument as given in Section 4.1.3 will be used here to determine which inlet temperatures are optimal for the SLIMR. To be able to reach higher powers while having a resilient flow, the maximum of the M vs P curve has to shift to the right in the power domain. This happens for lower inlet temperatures and is accompanied by an unwanted side-effect; the mass flow rate goes up as well and lowers the core outlet temperature. So again, a trade-off is made between a high power and a high core outlet temperature, and the scales are tipped in favor of a higher power. It is thus decided that the inlet temperature should lie somewhere in the range of 280 °C to 290 °C, because the $\frac{\mathrm{d}M}{\mathrm{d}P} \approx 0$ point of the M vs P curves lies right of 300 MW in Figure 4.1(c). Lower inlet temperatures also prevent higher thermal losses during nominal operation and enlarge the heat sink during accident scenarios, when the water has to absorb the decay heat.

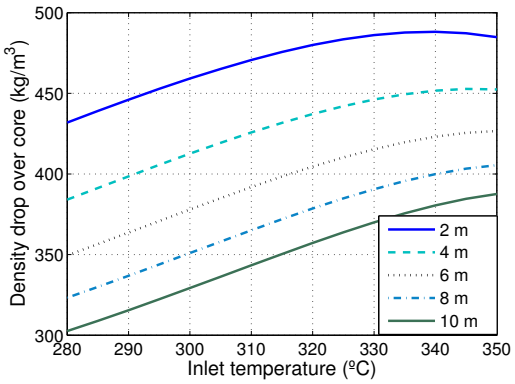

(a) Density drop over the core for P=150 MW and various riser lengths.

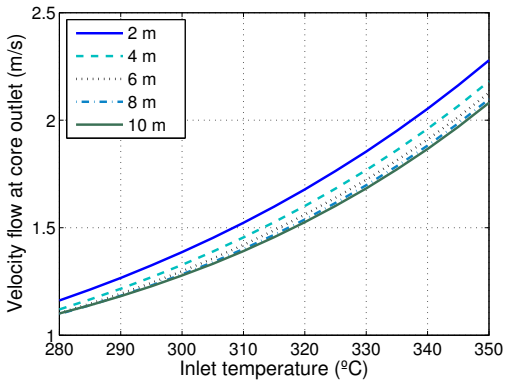

(b) Velocity of the fluid at the core outlet for P=150 MW and various riser lengths.

Figure 4.4: The influence of the inlet temperature on the density drop over the core and the velocity of the flow at the core outlet.

4.1.5 Variation of the power

Choosing a higher power is crucial for the financial performance of the SLIMR and therefore the desired range is on the high end; 300 to 350 MW. However, safety (and thus operational performance) is of paramount importance and therefore the operational point must lie around the maximum of the M vs P curve to ensure a stable flow. Figure 4.1(c) and 4.2(c) both show that this maximum lies at higher powers for low inlet temperatures and high risers. As a result, for lower inlet temperatures and higher risers the mass flow rate goes up (Figure 4.2(a) and 4.3(a)) and decreases the core outlet temperature, because the heat is transferred to more mass.

So here lies a trade-off. By operating at a higher power and around the maximum of the M vs P curve, a core outlet temperature above 400 °C is unfortunately not reached.

4.1.6 The optimised reactor characteristics

In the previous sections a suitable range for each parameter has been found that meets the conditions as best as possible, shown in Table 4.3. The stability analysis will be carried out with a set of chosen parameters within this range, see Table 4.3. With these parameters the SLIMR has a mass flow rate of 271 kg/s and an outlet temperature of 396 °C at nominal operation. The reactor thus surpasses the pseudo critical point and operates at a higher outlet temperature and higher power (350 MW) than the SLIMR design of Veling.

Table 4.3: Optimal range of the design parameters.

Parameter	Range	Chosen
K_{inlet}	-	30
L_R	8 m to 10 m	9 m
T_{in}	280 °C to 290 °C	280 °C
P	300 MW to 350 MW	350 MW

4.2 Neutronic evaluation of the SLIMR

This section evaluates the neutronic characteristics of the three-pass SLIMR core. First the criticality with respect to the fuel enrichment is explored, after which the power density profile in each heating section is determined and compared to the HPLWR core. Lastly, the reactivity feedback coefficients for the Doppler effect and the moderator density feedback are calculated and discussed.

4.2.1 Criticality of the three-pass SLIMR core

One of the aspects engineers have to consider in designing a nuclear reactor is the enrichment of the uranium in the fuel. In this section an indicative value for the enrichment of the uranium in the fuel UO_2 for the SLIMR is given. The reason for investigating the influence of the enrichment on the criticality of the reactor is that other parameters are fixed. The geometry and configuration of the core have been fixed and the density profile is also determined by the power density profile, so altering these to reach criticality is not an option. Furthermore, the reason to investigate this is the fact that small reactor cores need higher enrichment of the fuel, due to the larger neutron leakage. In some cases heavy water is used to increase the moderation and avoid higher enrichment values.

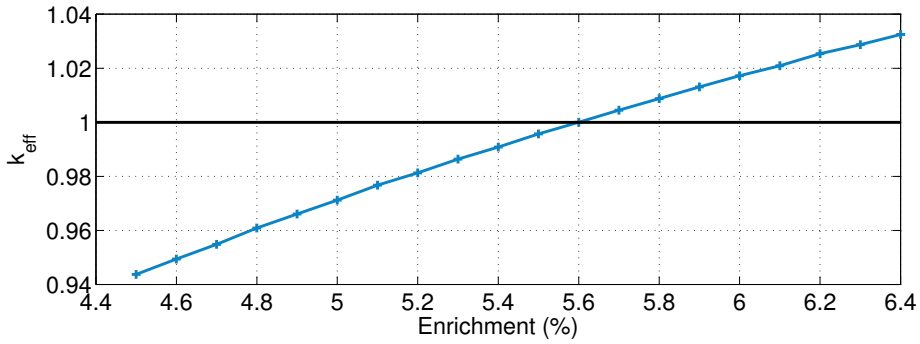

Figure 4.5: Effective multiplication factor as a function of enrichment. The reactor is critical, $k_{eff} = 1$, for an enrichment of 5.6 wt% UO_2.

Calculations on the effective multiplication factor of the SLIMR core have been done with *Serpent* for a range of enrichment values. At 5.6 wt% enrichment the reactor is critical as can be seen in Figure 4.5. This value is considered reasonable. It is slightly higher than the enrichment used in the other SMRs. The HPLWR incorporates various enrichment values for different clusters and these range between 3.0 to 7.0 wt%, so it is hard to compare this with the SLIMR core. Also, the SLIMR does not have moderator boxes as in the HPLWR fuel assemblies. This could lower the required enrichment value as more fuel material is located in each fuel assembly. Compared with the other type of SMRs discussed in the Section 1.1.2, 5.6 wt% is considered to be realistic in the case of the SLIMR.

4.2.2 Power distribution

One of the improvements on the SLIMR model is the incorporation of a more realistic power distribution than the original homogeneous distribution, which was a recommendation of Veling [36]. Because the power distribution scales with neutron density (see Eq. 2.18) the neutron density must be determined, which has been done with *Serpent* [18]. The neutron flux density in a reactor tends to be higher when

moderation of the neutrons is significant, resulting in a higher fission rate. In the SLIMR this occurs at nodes where the density of the moderator is high and thus foremostly in the Evaporator. Also, in the outer edges of the core the neutron flux density is low, due to leakage. Figure 4.6 shows the normalized power distribution as a function of the core height. As can been seen from the graph, the Evaporator accounts indeed for the largest part of the power followed by Superheater I. Superheater II produces the least amount of energy. What can also be made clear out of the graph is that the power is largest at the bottom of the core, where the density of the cold water is highest and thus moderation is significant. At the top of the core the neutron flux density is rather low due to the lower water density and the leakages at the edge of the core.

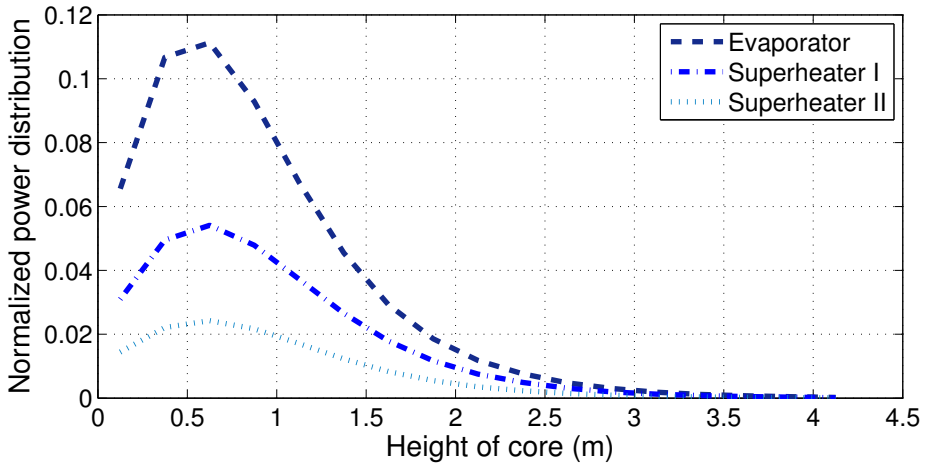

Figure 4.6: Normalized power distribution of the three sections in the SLIMR core.

A graphical interpretation of the cross-sectional distribution of the neutron flux density can be seen in Figure 4.7, a side view is given in Appendix A. The white and blue colors indicate the density of thermal neutrons and the red and yellow colors indicate where fission reactions take place. To confirm, the fuel pins are indeed colored red and yellow and in the water where moderation is high thermal neutrons are present.

This power distribution is compared to the power distribution in the HPLWR core to validate the results. Table 4.4 gives an overview of the absolute and relative power distribution in the three sections of the core of both reactors. The table shows that the relative power distribution is roughly the same for both reactors, only the Superheater II of the SLIMR produces a higher power than in the case of the HPLWR. This can be explained with the density profile of the HPLWR. The HPLWR reaches a significantly higher core outlet temperature and thus the Superheater II holds a coolant with a lower density, lowering its moderating capability and the fission rate in the outer heating section goes down.

Regarding the axial distribution the HPLWR has a more homogeneous distribution, see Figure 4.8. The discrepancy between the axial power distribution of the two reactors can be explained with the enrichment profiles. The enrichment of the fuel in the SLIMR is the same throughout the core, radially and axially, and does not compensate for the coolant density profile. This results in the drop in power after 2 meters in height, see Figure 4.6. In the case of the HPLWR the fuel has a higher enrichment in the upper half of the core. On average, the upper half of the fuel pins have an enrichment of 0.5 to 1 percentage point higher than the bottom half to account for the coolant density profile [32] and results in a flatter

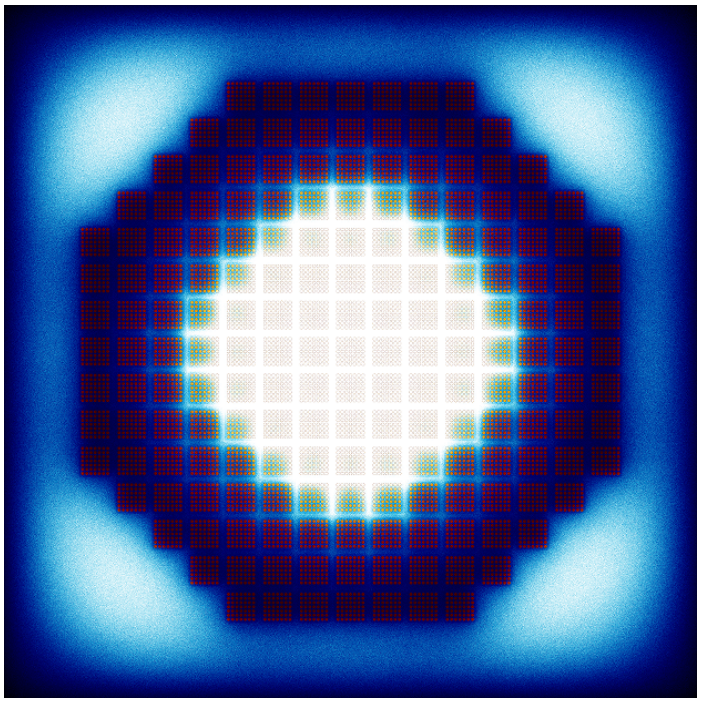

Figure 4.7: Graphical interpretation of the neutron flux density in the core. The red colors indicate where fission reactions occur and the white and blue colors indicate the presence of thermal neutrons. Image generated with *Serpent*.

axial power distribution (Figure 4.8). In the radial direction the HPLWR has an enrichment profile as well, but lies out of the scope of this research and will therefore not be explored here.

Table 4.4: The HPLWR and SLIMR power distribution. [32]

Core section	**HPLWR**	**SLIMR**
Total thermal power	2300 MW	350 MW
- Evaporator	1400 MW (60.9%)	199 MW (56.8%)
- Superheater I	800 MW (34.8%)	103.6 MW (29.6%)
- Superheater II	100 MW (4.3%)	47.4 MW (13.6%)

4.2.3 Reactivity feedback coefficients

An essential part of the coupling between the neutronics and the thermal hydraulics are the reactivity feedback coefficients. Section 3.2 discusses the approach to calculate the feedback coefficients for the Doppler effect and the moderator density feedback, the results are shown in Figure 4.9.

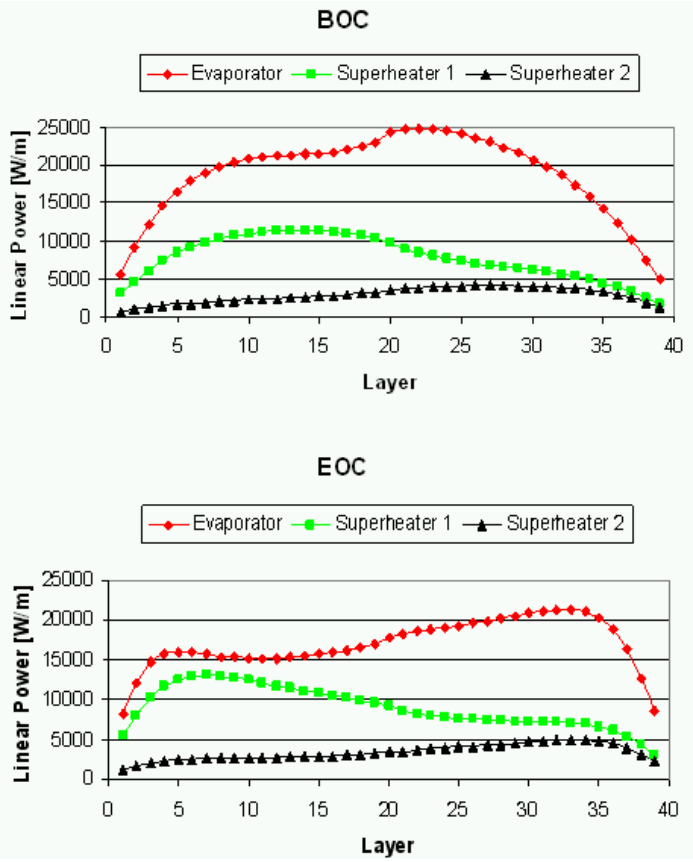

Figure 4.8: Axial power distribution of the HPLWR at the beginning of its life cycle (BOC) and at the end (EOC). Figure adopted from [32].

Moderator density feedback

The moderator density feedback coefficients are found to be in the range of 0.05 to 0.24 $(g/cm^3)^{-1}$, the numerical values are presented in the Appendix. For every node the coefficient is found to be positive and thus ensures a negative feedback mechanism. Compared to the values found by Schlagenhaufer et al. [30] the coefficients found for the SLIMR are approximately three to six times larger. They gave the following relation for the coolant density feedback of a fuel assembly of the HPLWR:

$$\alpha_\rho = -0.01424 \cdot \rho_{coolant} + 0.04236 \tag{4.1}$$

For the range of coolant densities in the SLIMR core this would lead to feedback coefficients in the order of $3 \cdot 10^{-2}$ to $4 \cdot 10^{-2}$ $(g/cm^3)^{-1}$, but the current *Serpent* calculations show the values are bigger. The difference between the values can be explained with the configuration of the fuel assemblies. As mentioned before the fuel assemblies of the SLIMR core are based on the HPLWR fuel assemblies, but lack a moderator box. The values found by Schlagenhaufer et al. are calculated for a change in coolant density at a fixed moderator density (the moderator fluid inside the moderator box). Thus the density for only a part of the surrounding fluid is changed and has therefore less impact than in the case of the SLIMR core, where the density of the entire coolant surrounding the fuel pins is changed. For this

reason the reactivity feedback coefficients are bigger than the ones found in the work of Schlagenhaufer et al. [30].

Doppler feedback

The fuel temperature feedback coefficients are found to be negative and in the range of $-3.5 \cdot 10^{-5}$ to $-1.5 \cdot 10^{-5}$ 1/K, with a few outliers in the upper section of the core. Negative coefficients are beneficiary for the stability of the reactor. Schlagenhaufer et al. [30] found values for the fuel temperature coefficient to range between $-1.5 \cdot 10^{-5}$ and $-2.0 \cdot 10^{-5}$, so the fuel temperature coefficients are of the same order of magnitude.

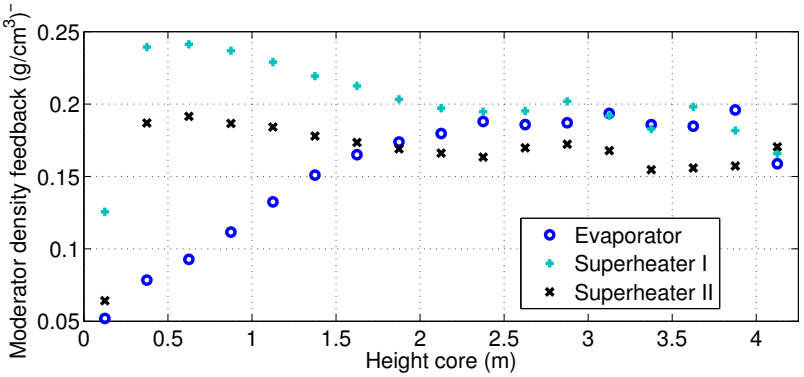

(a) Moderator density feedback coefficients for each heating section.

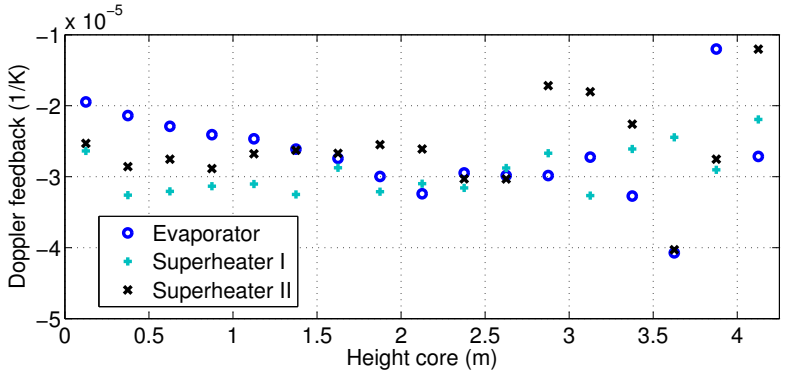

(b) Doppler feedback coefficients for each heating section.

Figure 4.9: The reactivity feedback coefficients for the SLIMR core. In total there are 51 nodes with a width of 0.25 m in the three heating sections.

Validation of the feedback coefficient approximation

To check whether the approximation of the reactivity feedback coefficients is valid one coefficient is begin evaluated. In this case the reactivity in one node has been calculated with *Serpent* for a range of densities. Node 4 has been chosen, where the steady state moderator density is equal to 0.597 g/cm^3. The results are shown in Figure 4.10 and show that the points form a slightly convex line. With the

method of least squares a first order fit is used to estimate the moderator density feedback coefficient in Node 4. The slope of the line is equal to 0.15 $(g/cm^3)^{-1}$ and is thus larger than the approximated value (0.11 $(g/cm^3)^{-1}$). This means the increase of 0.2 g/cm^3 is too big to estimate the feedback coefficient. It would be therefore better to use a density dependent relation for the moderator density coefficient, such as Eq. 4.1. This unfortunately requires more computational time to derive a relation for every node. Neglecting the spatial dependency would reduce the computational time, because only one node has to be evaluated for a range of densities. There would then be only one relation for the reactivity feedback coefficient for all the nodes, dependent on the density of the moderator. This works if all the nodes were identical, but when the shape and fuel composition of each node varies these numbers could vary for each node and one should make a decision which accuracy is more important.

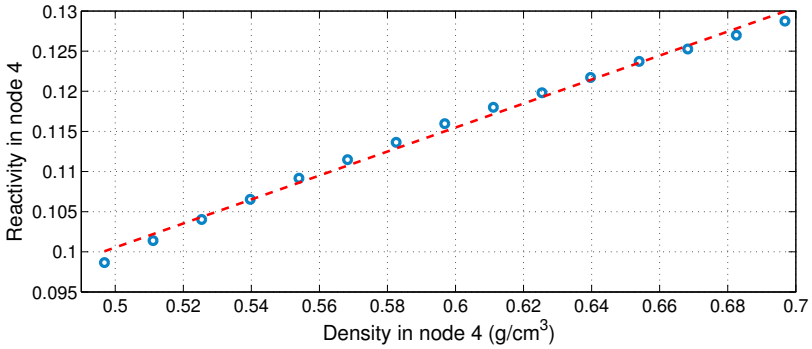

Figure 4.10: Reactivity for a range of densities in Node 4 of the SLIMR core, which is located between 0.75 and 1.00 m in the Evaporator section.

4.3 Stability

Coupling the neutronics to the thermal hydraulics of the reactor might reveal instabilities in the system. This chapter is dedicated to finding those instabilities. Veling [36] investigated the stability by introducing a 10% increase in power for 10 seconds and studying the response of the reactor afterwards with transients. To give an example of such a transient, Figure 4.11 shows the mass flow rate as a function of time of the SLIMR in Veling's work [36]. This graphs shows that the system recovers quickly towards the steady state. To compare this with the stability behaviour of the SLIMR in this research, where neutronics

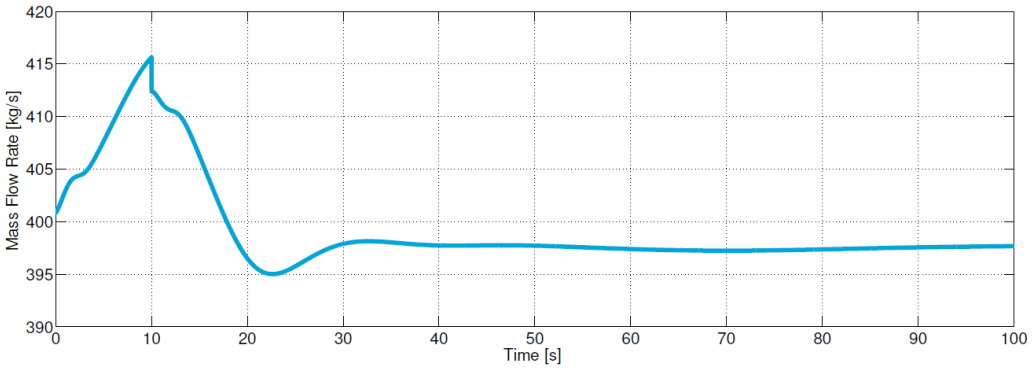

Figure 4.11: Response of the SLIMR in Veling's work after a perturbation of the power. Image adopted from [36].

are included, the system is perturbed with a reactivity insertion of 100 pcm throughout the core for 10 seconds. For the chosen parameters in Table 4.3 the response of the system is calculated and depicted in Figure 4.12. The power generated in the core (blue line) quickly rises due to the production of additional prompt neutrons as a result from the extra reactivity. Due to the delayed heat transfer (red line) the fuel temperature quickly rises as well and results in negative reactivity from the Doppler effect, lowering the generated power quickly. The system then tries to find a steady state until the reactivity insertion is removed (after 10 s) and the power drops. After a while the system recovers to its original steady state. From this graph it can be seen that the heat transfer delay is small and that it mainly smooths out large peaks in the generated power.

Figure 4.12(b) shows the response of the mass flow rate. The sudden increase of the heat transfer (red line) drives the mass flow rate up, but eventually the mass flow rate drops below under its steady state value (around t=5 s), while the heat transfer is still above its steady state value. This can be expected as the operational point lies to the right of the $\frac{\mathrm{d}M}{\mathrm{d}P} \approx 0$ point of the M vs P curve, where the mass flow rate drops for higher powers. In the end also the mass flow rate recovers to its original steady state value. So, for the chosen parameters the system is found to be stable. In fact, the system is found to be stable for a wide range of operational parameters. The power has been varied from 100 MW to 440 MW in steps of 20 MW and for each of these powers the inlet temperature has been varied from 250 °C to 350 °C in steps of 10 °C. Every operational point was found to be stable when an additional 100 pcm was introduced to the system.

To get an idea of the response of the SLIMR after a perturbation is introduced transients are analysed and a time decay constant with which the perturbation dies out is determined. This time decay constant must not be confused with the decay constant of the precursors. The time decay constant gives an idea when the system approaches an unstable regime. Large constants indicate the perturbation dies out quickly and

small constants indicate that the perturbation remains longer in the system. The next section explores the time decay constant when the delay between the heat transfer and the generated power in the core is varied. This has been done for various reactivity insertions, ranging from 0.1$ to 1$ (in steps of 0.1$), to see whether the model behaves linearly. Although the models are all linearised, the combination of the thermal-hydraulics and the neutronics model could lead to non-linear effects, due to the feedback between them. It has been found that the size of the perturbation changes proportional to the size of the reactivity insertions and that non-linear effects are thus not at play for the studied scenarios.

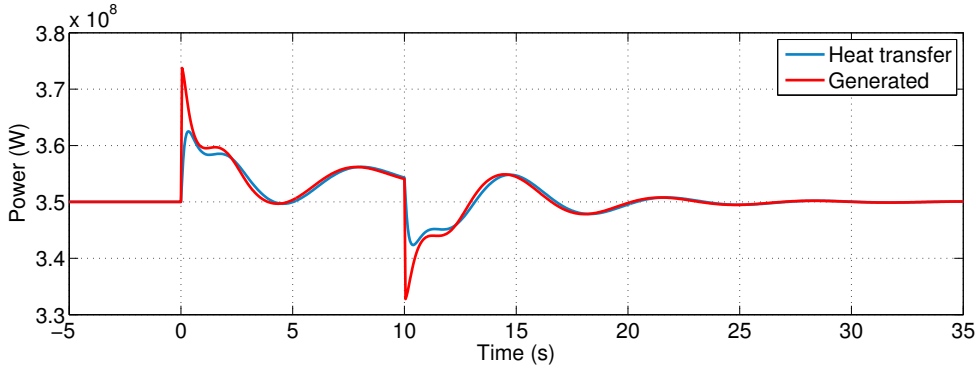

(a) Response of the power generated and heat transfer to the coolant as a response to a reactivity insertion of 100 pcm for 10 seconds with $D_{\text{pin}} = 8mm$.

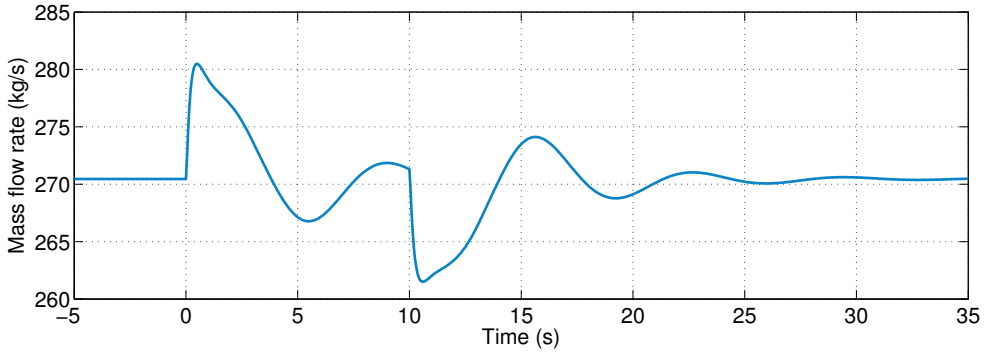

(b) The mass flow rate during a perturbation of the steady state. The system quickly recovers to its former state.

Figure 4.12: Response of the system, i.e. power, heat transfer and mass flow rate, after a perturbation.

4.3.1 Influence of the heat transfer delay on the system's response

A parameter that has been left out of the parameter study is the fuel pin diameter. This parameter has not been varied, because the aim was to stay as close as possible to the geometry of the HPLWR core. However, the pin diameter could have a influence on the delay of the heat transfer and thus on the stability of the system. Changing the fuel pin diameter does however change the steady state of the reactor significantly and for this reason an in-depth analysis of the fuel pin diameter is not pursued in this research. Appendix C shows some results and gives additional explanation on the influence of the fuel pin diameter. So, instead of varying the fuel pin diameter the heat transfer coefficient of the fuel pin's surface to the coolant has been varied to change the delay of the heat transfer. In this way the steady state operation of the reactor stays the same, but the response of the system with respect to perturbations changes. Without wondering if the coefficient is realistic the heat transfer coefficient is varied to study the influence on the response of the system.

The heat transfer coefficient of the fuel pins has an influence on the delay of the heat transfer. If the coefficient is large, heat dissipates quickly to the coolant and the heat transfer follows the generated power quickly. In this same line of reasoning, when the coefficient is small the fuel pin can not dissipate its heat quickly and the fuel pin temperature rises till the heat transfer matches the generated power. This introduces a delay of the heat transfer with respect to the generated power. This delay can cause perturbations to remain longer in the system and therefore the time decay constant of the system's response is determined.

Determining the time decay constant

After observing several transients of the system after a perturbation is introduced the response of the mass flow rate of the system can best be described with the following relation:

$$M(t) - M_{SS} = Ae^{-at}\cos(\theta + \omega t) \tag{4.2}$$

In this equation M represents the mass flow rate, a is the time decay constant of the perturbation, t is the time, A and θ represent the amplitude and phase shift of the perturbation. The time decay constant can be found by taking the ratio of the peaks of the response and cancelling out common terms.

$$\frac{M(t_2) - M_{SS}}{M(t_1) - M_{SS}} = \frac{Ae^{-at_2}\cos(\theta + \omega t_2)}{Ae^{-at_1}\cos(\theta + \omega t_1)} = \frac{e^{-a(t_1+\Delta t)}}{e^{-at_1}} = e^{-a\Delta t} \tag{4.3}$$

So by taking the coordinates of the maxima in the response the cosine is eliminated and after some basic algebra Eq. 4.4 is obtained. Figure 4.13 gives an example of the exponential approximation that is made and indicates the maxima in the response.

$$a = -\frac{\ln\left(\frac{M(t_2) - M_{SS}}{M(t_1) - M_{SS}}\right)}{\Delta t} \tag{4.4}$$

This means that for large values of a the system is considered more stable and for low values of a the system is less stable, as it takes longer for perturbations to die out. If a becomes negative, the system is considered unstable, but these instabilities have not been found in this research.

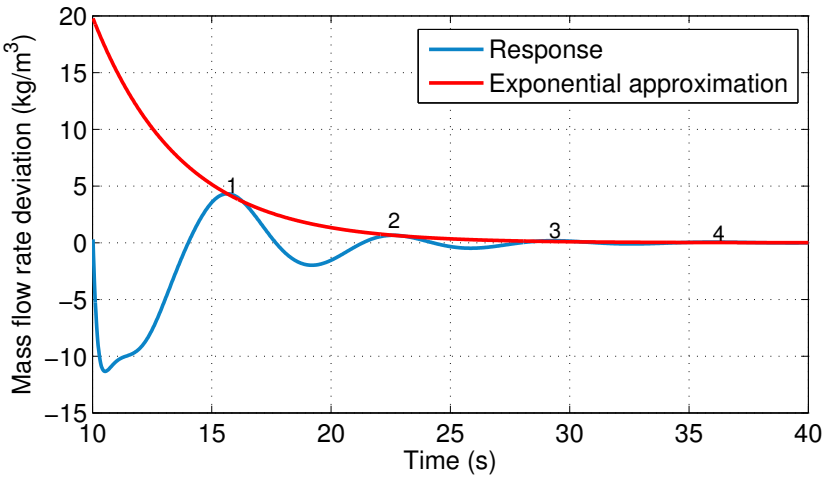

Figure 4.13: Response of the SLIMR after a perturbation. The deviation of the mass flow rate with respect to the steady state value is plotted. The numbers indicate maxima of the response.

Varying the heat transfer coefficient

With the Dittus-Boelter equation (Eq. 2.23) the steady state value of the heat transfer coefficient of the fuel pin's surface to the coolant ranges between $2 \cdot 10^4$ and $4 \cdot 10^4$ W/m^{2}K, depending on the position in the core. The heat transfer coefficient has been varied from $2.5 \cdot 10^3$ W/m^{2}K to $6 \cdot 10^4$ W/m^{2}K in steps of $2.5 \cdot 10^3$ W/m^{2}K. The chosen range therefore explores values below and above the range in the model. For every response the time decay constant is determined with the previous mentioned method and the results are plotted in Figure 4.14 for three different operational points.

To compare various stability maps of different reactors dimensionless numbers are introduced, which are a measure of two operational parameters; inlet temperature and power. These numbers are the pseudo phase change number, N_{pch}, and the subcooling number N_{sub} and are given in Eq. 4.5 and Eq. 4.6 respectively. These dimensionless numbers[4] are also used in the work of T'joen and Rohde [33] to display their stability map for the DeLight facility. The results in this research are qualitatively compared to their results. The resulting stability map is shown in Figure A.1 in the Appendix.

$$N_{pch} = \frac{P}{M h_{pc}} \tag{4.5}$$

$$N_{sub} = \frac{h_{pc} - h_{in}}{h_{pc}} \tag{4.6}$$

Let us consider first the blue line, which holds for the SLIMR with $T_{in} = 280\,^{\circ}$C and $P = 350$ MW as chosen in Section 4.1. The graph confirms the presumption that lower values of the heat transfer coefficient lower the time decay constant and lead the system towards the unstable regime (if there is an unstable regime). This can be explained by considering the delay of the heat transfer. If heat is transferred at a later time than that it is generated the moderator density feedback is delayed as well with

[4] Though slightly different presented here.

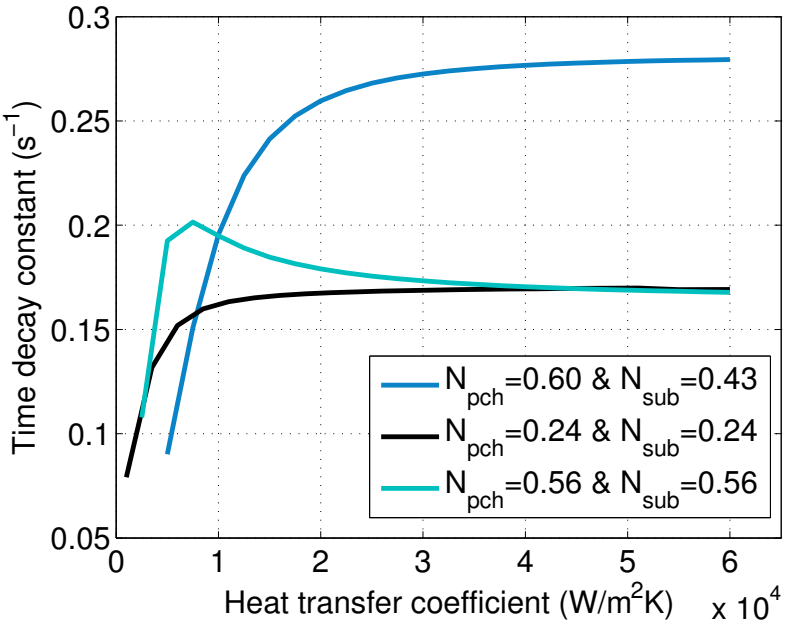

Figure 4.14: Time decay constant against the heat transfer coefficient of the fuel pin's surface to the coolant for three different operational points.

respect to the fuel temperature feedback, which takes effect directly. These two feedback mechanisms are then out of phase and result in a less stable system.

Figure 4.15 shows two graphs in which the difference between two responses of the system is significant. For a smaller heat transfer coefficient (Figure 4.15(b)) the reactivity insertion (0.5$) leads to higher excursions of the power and the system takes longer to return to its original state. Whereas the system with a larger heat transfer coefficient (Figure 4.15(a)) has a smaller power excursion and the perturbation dies out sooner. From the three operational points studied the time decay constant is higher for the $N_{pch} = 0.60$ and $N_{sub} = .43$ operational point and thus indicates a more stable system. This does however not agree with the results found by T'Joen and Rohde [33], as their system is highly unstable for $N_{pch} = 0.60$ and $N_{sub} = .43$, see Figure A.1.

Regarding the other two graphs in Figure 4.14, they show similar results for lower heat transfer coefficients, i.e. a less stable system. The dimensionless numbers of these operational points are equal to each other and indicate that the core outlet temperature lies at the pseudo-critical point. These operational points are interesting, because the thermophysical properties of supercritical water at the pseudo-critical point vary significantly. For the $N_{sub} = 0.24$ case (where the core inlet temperature is high) lower time decay constants are found than the $N_{sub} = 0.24$, indicating a less stable system. The same holds for the $N_{sub} = 0.56$ graph. Only in this graph the time decay constant increases slightly before dropping when the heat transfer coefficient becomes smaller, why this happens is unclear at this moment. Figure A.1 does not show results for the $N_{sub} = 0.56$ case, but it is found that for the $N_{sub} = 0.24$ case the system lies near the neutral stability line[5] and is found to be more stable (or less unstable) than the $N_{pch} = 0.60$

[5]The neutral stability line indicates operational points where the perturbation in the system does not die out or grow.

and $N_{sub} = .43$ case. This is contrary to what is found here. Though, it has to be mentioned that comparing these results with the stability maps of T'Joen and Rohde is cumbersome, as both the systems are different and that in this research no instabilities were found at all.

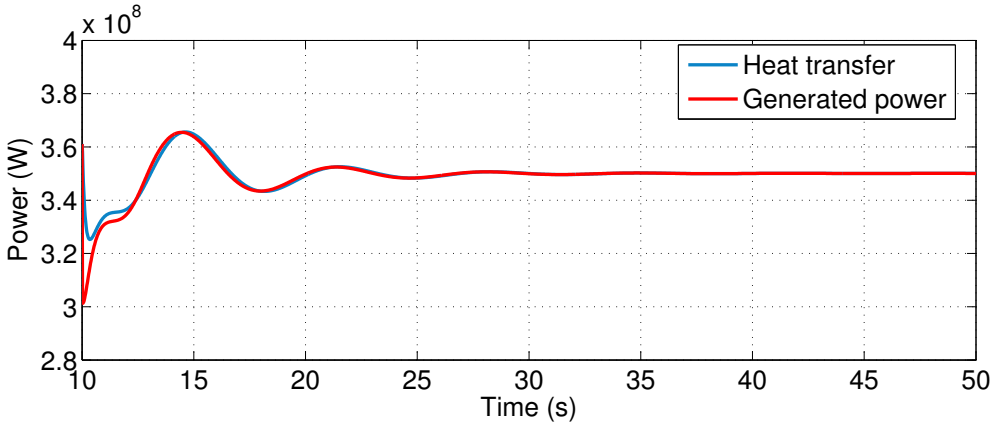

(a) Response of the power generated and heat transfer to the coolant as a response to a reactivity insertion of 0.5$ for 10 seconds with $h = 4 \cdot 10^4$ W/m^{2}K. Time decay constant is 0.28 s^{-1}.

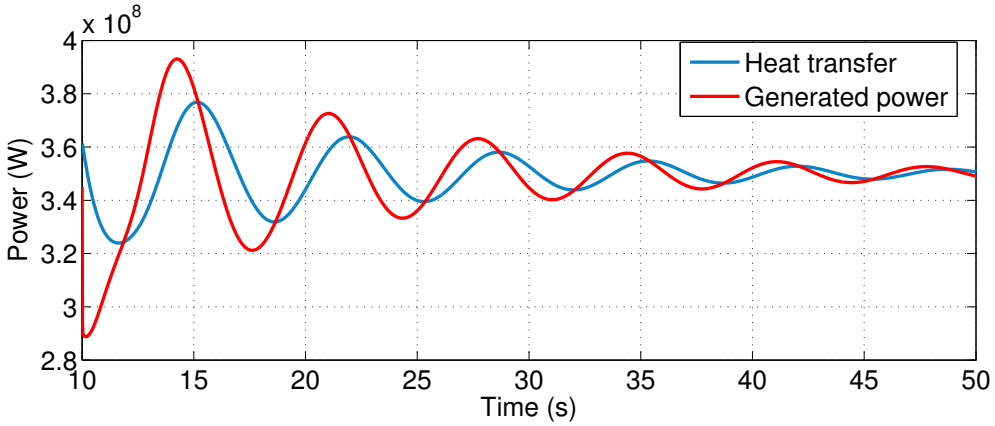

(b) Response of the power generated and heat transfer to the coolant as a response to a reactivity insertion of 0.5$ for 10 seconds with $h = 5 \cdot 10^3$ W/m^{2}K. Time decay constant is 0.09 s^{-1}.

Figure 4.15: Response of the system. For lower values of the heat transfer coefficient the delay of the heat transfer with respect to the generated power increases and causes the system to take longer to return to its original state.

Chapter 5

Conclusions and Recommendations

Veling [36] has made the first steps towards a design of a supercritical water SMR driven by natural convection. He showed that the design of the SLIMR has potential with respect to safety and stable passive operation, by investigating both normal and accidental situations. For example, decay heat could be passively transported to the surrounding pool in the event of a SCRAM accompanied by a station blackout (if the coolant temperature did not exceed 385 °C). However, his design did not surpass the critical temperature of 374 °C, making it in fact a light water reactor without exploiting the advantages of surpassing the pseudo-critical temperature. Also his design operated at a relative low thermal power of 150 MW and when considering the stability of the system neutronics were left out. The research at hand was aimed at overcoming these shortcomings and its conclusions are presented here, followed by recommendations for future work.

5.1 Conclusions

On the basis of the sub-questions stated in Section 1.4 the main research question is answered. First of all, the one-pass core design of Veling [36] has been substituted by a three-pass core design based on the HPLWR core. This core design enabled the reactor to operate at a higher power and higher core outlet temperature. From the parameter study performed with the updated SLIMR model optimal design parameters to increase the performance of the SLIMR have been found, while considering the constraint of a stable system. By incorporating a riser with a length ranging between 8 m and 10 m and setting the core inlet temperature between 280 °C and 290 °C a significant higher power of 350 MWth can be achieved, in comparison with 150 MWth in Veling's work [36]. This operational point reaches a core outlet temperature of 396 °C and thus surpasses the pseudo-critical point and increases the efficiency.

Secondly, the three-pass core design has been evaluated on its neutronic characteristics by Monte-Carlo calculations. The UO_2 in the fuel pins has to have an enrichment of 5.6 wt% to ensure a critical core. Furthermore, the constant axial power profile of Veling [36] has been updated with a more realistic profile in both the axial and radial direction by studying the neutron density inside the core. This power profile is crucial for the evaluation of heat deterioration in the core, because in high neutron flux regions the heat transfer is greater and could lead to a deteriorated heat transfer coefficient. However, by resting on the work done for the three-pass core design of the HPLWR heat transfer deterioration is assumed not

to occur. Furthermore, reactivity feedback coefficients for the Doppler feedback and moderator density feedback were determined and ensure negative feedback mechanisms between the neutronics and the thermal hydraulics of the SLIMR.

With these reactivity feedback coefficients the stability of the reactor has been studied and for the chosen parameters the SLIMR is found to be stable. By varying the heat transfer coefficient of the fuel pin's surface to the coolant the delay of the heat transfer with respect to the generated power can be influenced and it has been shown that lower values of the heat transfer coefficient cause perturbations to remain longer in the system, indicating a tendency of the system to go towards an unstable state.

To conclude, by incorporating a three-pass core design the reactor performance with respect to power and efficiency can be increased. Expanding the SLIMR model with a nodal kinetics model to include feedback mechanisms made the model more realistic and no instabilities were found during simulation. However, attention must be given towards the heat transfer coefficient of the fuel pins as it can contribute to a more unstable state of the SLIMR. Heat transfer deterioration is therefore a phenomenon that must be avoided, because it lowers the heat transfer coefficient significantly.

5.2 Recommendations

This research continued with the recommendations (not all) Veling [36] made for future research. Though, while this research has set a next step with the SLIMR design, much can still be done in future work.

First of all, the axial power profile can be improved. In the current research most of the power is generated in the lower part of the core, because the density of the moderator is highest in this region. In general a more flattened axial power profile is desired to ensure a certain homogeneous burn-up of the fuel throughout the core. In the HPLWR design this is solved by increasing the enrichment in the upper sections of the core. A similar method could be applied for the SLIMR core. Continuing on the fuel aspect of the SLIMR, it is also recommended to study the burn-up throughout its operation cycle. The burn-up changes the power profile inside the core over time and on its turn changes the axial density profile and thus the level of moderation. Potential local power peaks could then be discovered, which leads to the second recommendation.

Secondly, this research has shown that the heat transfer coefficient of the fuel pin's surface to the coolant is an important parameter with respect to the stability of the system and research for the HPLWR has shown that heat transfer deterioration is important to take into account. It is therefore recommended to build a 2-dimensional (in the axial and radial direction) thermalhydraulic model for the water loop combined with a radial dependent conduction model over each fuel rod element to study the heat transfer from the fuel rods to the coolant. By doing so the internal heat transfer coefficient of the fuel rod as well as the heat transfer coefficient to the coolant can be accurately modeled. A more realistic approximation for the outer heat transfer coefficient, instead of the Dittus-Boelter relation, could be incorporated. For example, the altered version of the Krasnoshchekov-Protopopov correlation, as proposed in the work on the HPLWR [32], can be used. By developing the 2-dimensional model the process of laminarisation near the fuel rods (Section 2.2) could be modeled to study potential hot spots in the core (which could put stress on the materials). By introducing a more flattened axial power profile, as just recommended, these hot spots could be avoided, but it is up to future research to validate this claim.

Thirdly, Veling [36] recommended to design a second containment surrounding the RPV, in which a vacuum is maintained, to lower the heat loss during nominal operation. However, during accident scenarios this containment should be filled passively with a coolant to remove the decay heat. This research did not look into this aspect of the design, but future research could explore solutions to the heat loss during

nominal operation. A solution could be to design a second containment, which is connected through an inverted siphon with the surrounding pool. Pumps would maintain a sufficient air pressure inside the second containment to keep the water outside of the containment and reduce heat loss during nominal operation. As soon as there is an accident (accompanied by a power outage), pumps will shut-off and the elevated air pressure falls away. The water of the pool then streams into the second containment, cooling down the system. The SLIMR model could be expanded with this second containment and calculations can be done to see if this solution reduces the heat loss during nominal operation and is capable of removing the decay heat during accident scenarios.

Lastly, the SLIMR design has a three-pass core design in which Superheater I has a downward flow, but the density difference over this section imposes a counteracting buoyancy force. During nominal operation this is not a problem, but during start-up situations and during SCRAM scenarios followed by a station blackout this could result in a reversed flow. This might have implications for the stability and safety of the reactor, but these scenarios have not been explored here and could be addressed in future work.

Bibliography

[1] Atomic Power Review. SMART SMR moves ahead - in saudi arabia and at home. "http://atomicpowerreview.blogspot.nl/2015/03/smart-smr-moves-ahead-in-saudi-arabia.html, 2015 (accessed September 11, 2015).

[2] Babcock & Wilcox Enterprises, Inc. B&W announces restructuring of small modular reactor program. "http://www.babcock.com/news-room/Pages/BW-Announces-Restructuring-of-Small-Modular-Reactor-Program.aspx, 2015 (accessed July 22, 2015).

[3] Kyoo Hwan Bae, Hee Cheol Kim, Moon Hee Chang, and Suk Ku Sim. Safety evaluation of the inherent and passive safety features of the SMART design. *Annals of Nuclear Energy*, 28(4):333 – 349, 2001.

[4] Young-Jong Chung, Seong Wook Lee, Soo Hyoung Kim, and Keung Koo Kim. Passive cooldown performance of a 65 MW integral reactor. *Nuclear Engineering and Design*, 238(7):1681 – 1689, 2008.

[5] Z. Dong, X. Huang, and L. Zhang. A nodal dynamic model for control system design and simulation of an MHTGR core. *Nuclear Engineering and Design*, 240(5):1251 – 1261, 2010.

[6] M.O. McLinden E.W. Lemmon and D.G. Friend. *Thermophysical Properties of Fluid Systems*. National Institute of Standards and Technology, 2015.

[7] F. Frieß, M. Kütt, and M. Englert. Proliferation issues related to fast SMRs. *Annals of Nuclear Energy*, 85:725 – 731, 2015.

[8] T. Ortega Gomez. *Stability analysis of the high performance light water reactor*. PhD thesis, TIB Hannover, March 2009.

[9] J. A. Halfinger and M. D. Haggerty. The B&W mPower Scalable, Practical Nuclear Reactor Design. *Nuclear Technology*, 178:164 – 169, 2011.

[10] H. Hidayatullah, S. Susyadi, and M. Hadid Subki. Design and technology development for small modular reactors - Safety expectations, prospects and impediments of their deployment. *Progress in Nuclear Energy*, 79:127 – 135, 2015.

[11] D.T. Ingersoll, Z.J. Houghton, R. Bromm, and C. Desportes. Nuscale small modular reactor for co-generation of electricity and water. *Desalination*, 340:84 – 93, 2014.

[12] G. Iyer, N. Hultman, S. Fetter, and S.H. Kim. Implications of small modular reactors for climate change mitigation. *Energy Economics*, 45:144 – 154, 2014.

[13] J.D. Jackson. Fluid flow and convective heat transfer to fluids at supercritical pressure. *Nuclear Engineering and Design*, 264:24 – 40, 2013. SI:NURETH-14.

[14] T. Jevremovic. *Nuclear Principles in Engineering*. Springer Science+Business Media, Inc., 2005.

[15] F. Kam. Development of a one-dimensional model for the stability analysis of a natural circulation Super Critical Water Reactor, June 2011.

[16] H. Koopman. Development of the stealth-code and investigation of the effects of feedwater sparger positioning on the thermal-hydraulic stability of natural circulation boiling water reactors, June 2008.

[17] D. Krijger. A linear stability analysis of a water loop driven by natural convection at supercritical conditions, July 2013.

[18] J. Leppänen. *Serpent - a Continuous-energy Monte Carlo Reactor Physics Burnup Calculation Code*. VTT Technical Research Centre of Finland, March 2013.

[19] Zhitao Liu and Jihong Fan. Technology readiness assessment of small modular reactor (SMR) designs. *Progress in Nuclear Energy*, 70:20 – 28, 2014.

[20] G. Locatelli, C. Bingham, and M. Mancini. Small modular reactors: A comprehensive overview of their economics and strategic aspects. *Progress in Nuclear Energy*, 73:75 – 85, 2014.

[21] G. Locatelli, S. Boarin, F. Pellegrino, and M.E. Ricotti. Load following with small modular reactors (SMR): A real options analysis. *Energy*, 80:41 – 54, 2015.

[22] L. Paparusso, M. Ricotti, and M. Sumini. World status of the SMR projects. 2011.

[23] B. Pershagen. *Light water reactor safety*. Pergamon Press, 1989.

[24] I. L. Pioro and R. B. Duffey. Experimental heat transfer in supercritical water flowing inside channels (survey). *Nuclear Engineering and Design*, 235(22):2407 – 2430, 2005.

[25] I. L. Pioro, H. F. Khartabil, and R. B. Duffey. Heat transfer to supercritical fluids flowing in channels-empirical correlations (survey). *Nuclear Engineering and Design*, 230(1-3):69 – 91, 2004. 11th International Conference on Nuclear Energy.

[26] T. Reiss, S. Fehér, and Sz. Czifrus. Coupled neutronics and thermohydraulics calculations with burn-up for HPLWRs. *Progress in Nuclear Energy*, 50(1):52 – 61, 2008.

[27] M. Rohde. *Safe and sustainable nuclear energy: the Thorium-based small, modular, supercritical water reactor*. VIDI proposal, 2012.

[28] M. Rohde, C.P. Marcel, C. T'Joen, A.G. Class, and T.H.J.J. van der Hagen. Downscaling a supercritical water loop for experimental studies on system stability. *International Journal of Heat and Mass Transfer*, 54(1-3):65–74, 2011.

[29] M. K. Rowinski, T. J. White, and J. Zhao. Small and medium sized reactors (SMR): A review of technology. *Renewable and Sustainable Energy Reviews*, 44:643 – 656, 2015.

[30] M. Schlagenhaufer, B. Vogt, and T. Schulenberg. Reactivity control mechanisms for a HPLWR fuel assembly. In *Global 2007*.

[31] J. Spoelstra. Numerical stability analysis of natural circulation driven supercritical water reactors, December 2012.

[32] J. Starflinger. Public final report - assessment of the HPLWR concept. Technical report, Karlsruhe Institute of Technology, 2010.

[33] C. T'Joen and M. Rohde. Experimental study of the coupled thermo-hydraulic-neutronic stability of a natural circulation HPLWR. *Nuclear Engineering and Design*, 242(0):221 – 232, 2012.

[34] N. Todreas. Chapter 1 - Small modular reactors (SMRs) for producing nuclear energy: an introduction. In M.D. Carelli and D.T. Ingersoll, editors, *Handbook of Small Modular Nuclear Reactors*, Woodhead Publishing Series in Energy, pages 3 – 26. Woodhead Publishing, 2015.

[35] N. Town and S. Lawler. 12 - Construction methods for small modular reactors (SMRs). In M. D. Carelli and D. T. Ingersoll, editors, *Handbook of Small Modular Nuclear Reactors*, Woodhead Publishing Series in Energy, pages 293 – 317. Woodhead Publishing, 2015.

[36] D. Veling. The Small-scale Large efficiency Inherent safe Modular Reactor, November 2014.

[37] Yu.V. Vikhrev, A.S. Kon'kov, and Yu.D. Barulin. A study of heat transfer in vertical tubes at supercritical pressures. *Thermal Engineering*, 14(9):116 – 119, 1967.

[38] Yu.V. Vikhrev, A.S. Kon'kov, V.A. Lokshin, and et al. Temperature regime of steam generating tubes at supercritical pressure. In *Transactions of the IVth All-Union Conference on Heat Transfer and Hydraulics at Movement of Two-Phase Flow inside Elements of Power Engineering Machines and Apparatuses*, pages 21 – 40, Leningrad, Russia, 1971.

[39] C. L. Waata. *Coupled Neutronics/Thermal-hydraulics Analysis of a High-Performance Light-Water Reactor Fuel Assembly*. PhD thesis, Institut für Kern- und Energietechnik, July 2006.

[40] World Nuclear Association. Small nuclear power reactors. "`http://www.world-nuclear.org/info/Nuclear-Fuel-Cycle/Power-Reactors/Small-Nuclear-Power-Reactors/`, 2015 (accessed July 22, 2015).

[41] World Nuclear News. Saudi arabia teams up with korea on SMART. "`http://www.world-nuclear-news.org/NN-Saudi-Arabia-teams-up-with-Korea-on-SMART-0403154.html`, 2015 (accessed July 22, 2015).

[42] M. Yetisir, J. Pencer, M. McDonald, M. Gaudet, J. Licht, and R. Duffey. The Supersafe Reactor: A small modular pressure tube SCWR. *AECL Nuclear Review*, 1(2):13–18, 2012.

Appendix A

Additional figures

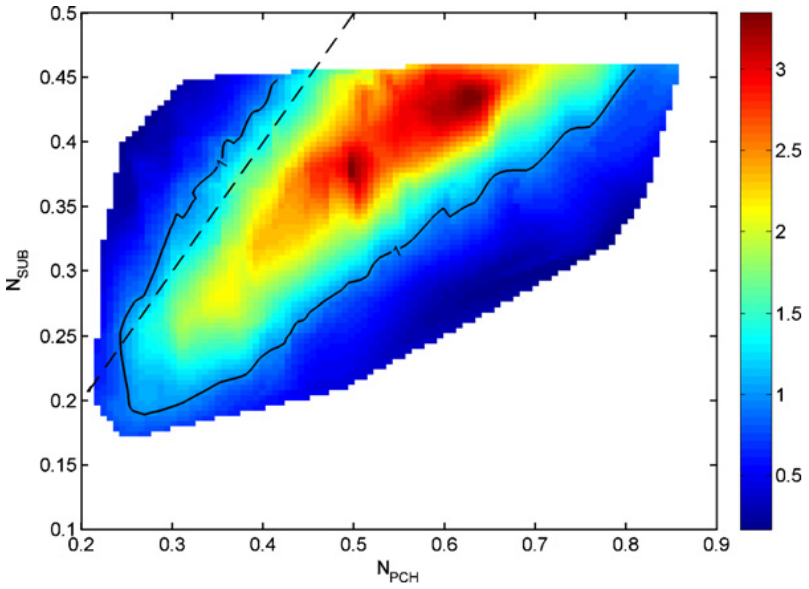

Figure A.1: Stability map for the Delight facility. Values above 1 indicate an unstable system, values below 1 indicate an unstable system. Figure adopted from T'Joen and Rohde [33]. The black line indicates a decay ratio of 1, the neutral stability line. The dashed line indicates where the exit temperature is equal to the pseudo-critical value.

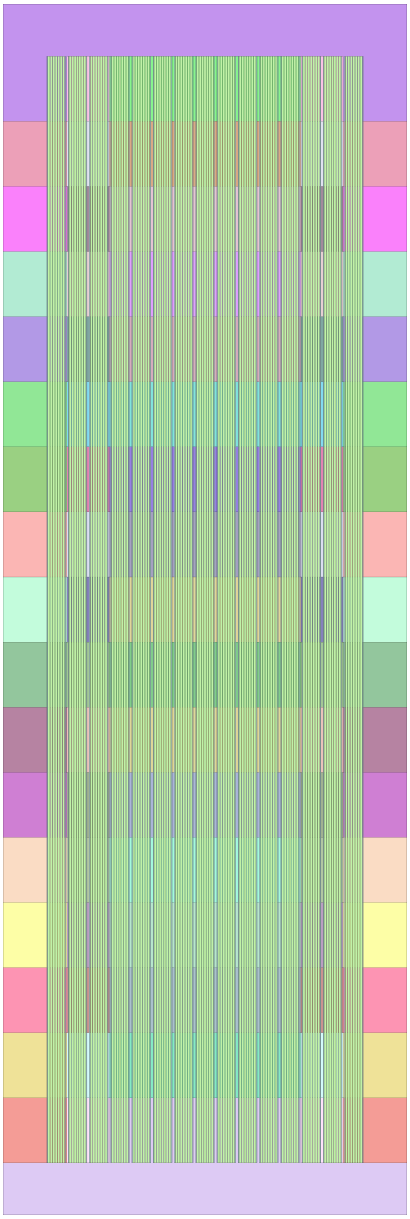

(a) Sideview of the SLIMR core configuration. The different colors indicate different materials with different temperatures. The core is divided into seventeen nodes and is 4.25 m high.

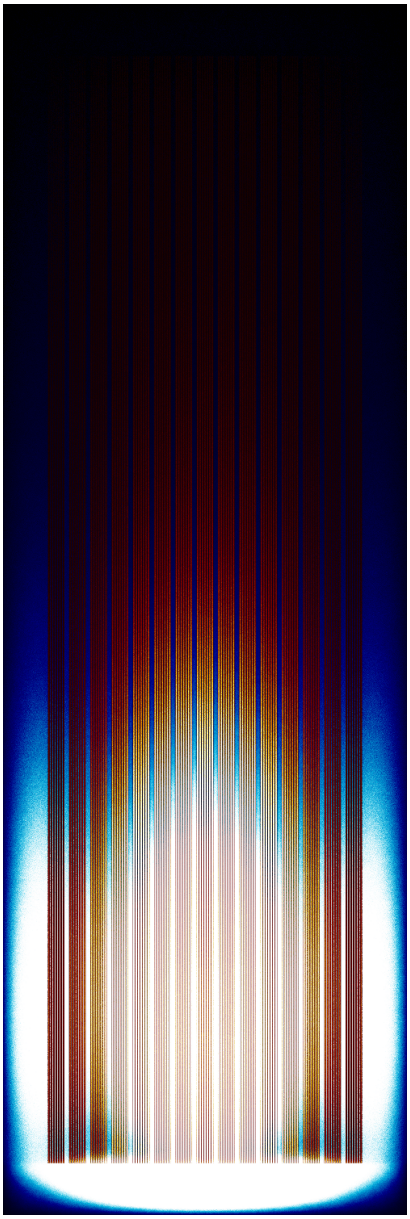

(b) Graphical interpretation of the neutron flux from a side view. White and blue colors indicate the presence of thermal neutrons and red and yellow indicate fission reactions. Image generated with *Serpent* [18].

Figure A.2: Side view of the three-pass core configuration.

Appendix B

Serpent and core characteristics

B.1 Core parameters

The parameters and materials used in the core setup for *Serpent* are given in Table B.1. A graphical interpretation of this core setup is given in Figure 3.1.

Table B.1: Geometry of the SLIMR core. Data comes partially from [32].

Core design	**Value**	**Unit**
Thermal power	350	MW
Height	4.25	m
Equivalent diameter	1.37	m
Fuel assemblies		
Number of fuel assemblies	185	-
- Evaporator	57	-
- Superheater I	64	-
- Superheater II	64	-
Assembly box inner side length	67.52	mm
Assembly box wall thickness	3	mm
Assembly box outer size	73.52	mm
Assembly box inner corner radius	2.5	mm
Assembly box outer corner radius	5.5	mm
Gap between assemblies	9	mm
Material assembly box	SS 347	-
Fuel pins		
Cladding inner diameter	7	mm
Cladding thickness	0.5	mm
Cladding alloy	SS 1.4970	-
Pitch	9.44	mm
Fuel	UO_2	-

B.2 *Serpent* options

Several options have to be set in the input file for *Serpent* to determine what to do. One of these options is the definition of the boundary condition for the neutrons, meaning what to do when neutrons reach the boundary of the geometry. There are three different settings; reflective, periodic and black. The setting in this case is set on "black", meaning that neutrons which pass the boundary are lost. The other two settings would imply that neutrons come back from outside the system and this is not the case here. Another setting to be defined is the number of active and inactive cycles to run. Also the number of source neutrons to run per cycle have to be defined. From early calculations it became clear that the accuracy is highly dependent on the number of active cycles and neutrons per cycle, which can be explained with the fact that *Serpent* is a Monte Carlo N-Particle based code [18]. In general the settings have been set to 9,000 active cycles with 40,000 neutrons per cycle. This increases the computational time significantly (up to 90 hours per calculation), but is necessary to calculate the reactivity feedback coefficients with enough accuracy, such that in a next run similar values are obtained. Table B.2 gives an overview of a few options.

Table B.2: Options for the SLIMR geometry.

Options	**Value**
Boundary condition	Black
Neutrons per cycle	40,000
Active cycles	9,000
Inactive cycles	40
Power	350 MW

B.3 Reactivity feedback coefficients

Table B.3: The values for the reactivity feedback coefficients for every node in the core, calculated with *Serpent* [18].

	Moderator density coefficient (g/cm^3)$^{-1}$			**Fuel temperature coefficient (1/K)**		
Height (m)	Evaporator	Superheater I	Superheater II	Evaporator	Superheater I	Superheater II
0.00-0.25	0.05	0.13	0.06	-1.9E-05	-2.6E-05	-2.5E-05
0.25-0.50	0.08	0.24	0.19	-2.1E-05	-3.3E-05	-2.9E-05
0.50-0.75	0.09	0.24	0.19	-2.3E-05	-3.2E-05	-2.8E-05
0.75-1.00	0.11	0.24	0.19	-2.4E-05	-3.1E-05	-2.9E-05
1.00-1.25	0.13	0.23	0.18	-2.5E-05	-3.1E-05	-2.7E-05
1.25-1.50	0.15	0.22	0.18	-2.6E-05	-3.3E-05	-2.6E-05
1.50-1.75	0.17	0.21	0.17	-2.7E-05	-2.9E-05	-2.7E-05
1.75-2.00	0.17	0.20	0.17	-3.0E-05	-3.2E-05	-2.5E-05
2.00-2.25	0.18	0.20	0.17	-3.2E-05	-3.1E-05	-2.6E-05
2.25-2.50	0.19	0.19	0.16	-2.9E-05	-3.2E-05	-3.0E-05
2.50-2.75	0.19	0.20	0.17	-3.0E-05	-2.9E-05	-3.0E-05
2.75-3.00	0.19	0.20	0.17	-3.0E-05	-2.7E-05	-1.7E-05
3.00-3.25	0.19	0.19	0.17	-2.7E-05	-3.3E-05	-1.8E-05
3.25-3.50	0.19	0.18	0.15	-3.3E-05	-2.6E-05	-2.3E-05
3.50-3.75	0.18	0.20	0.16	-4.1E-05	-2.4E-05	-4.0E-05
3.75-4.00	0.20	0.18	0.16	-1.2E-05	-2.9E-05	-2.8E-05
4.00-4.25	0.16	0.17	0.17	-2.7E-05	-2.2E-05	-1.2E-05

Appendix C

The influence of the fuel pin diameter on the system's response

In Figure C.1 the steady state mass flow rate and core outlet temperature are shown for a range of fuel pin diameters. It is important to keep the amount of fuel constant when varying the fuel pin diameter, to keep the power density constant. This means that when the fuel pin diameter is increased, the number of fuel pins inside the fuel assembly decreases quadratically. The wetted perimeter of the fuel assembly goes down and decreases the friction. This results in a greater mass flow rate and lower core outlet temperatures as can be seen in Figure C.1.

$$D_{pin} \Uparrow \quad \longrightarrow \quad P_w \Downarrow \quad \longrightarrow \quad \Delta p_{\text{friction}} \Downarrow \quad \longrightarrow \quad M \Uparrow \quad \longrightarrow \quad T_{\text{out}} \Downarrow$$

As said before a larger fuel pin diameter increases the delay of the heat transfer of the fuel pins with respect to the generated power. The delay is larger due to the larger volume of the fuel pin accompanied by a relatively smaller surface to exchange heat with the coolant. The heat flux through the surface has to be higher than for fuel pins with a smaller diameter, because more heat has to be dissipated. The fuel temperature has to increase to ensure a larger heat flux and this takes time. Also the internal heat transfer plays a role when varying the fuel pin diameter, but this heat transfer has not been modeled and its effect is therefore not reflected in the results. An example of the response of the system with a fuel pin diameter of 32 mm is given in Figure C.2. Comparing Figure C.2 with Figure 4.12(a) it can be seen that for a larger diameter the heat transfer has a bigger delay, but the system still returns to its steady state rather quick. For the range of 4 mm to 32 mm for the fuel pin diameter the system is found to be stable.

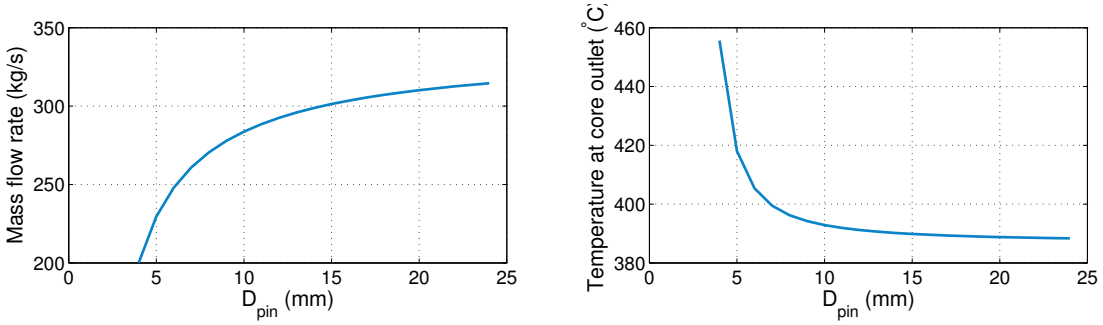

(a) Mass flow rate for a range of fuel pin diameters with the SLIMR geometry parameters in Table 4.3.

(b) Core outlet temperature for a range of fuel pin diameters with the SLIMR geometry parameters in Table 4.3

Figure C.1: Steady state behaviour with respect to the fuel pin diameter.

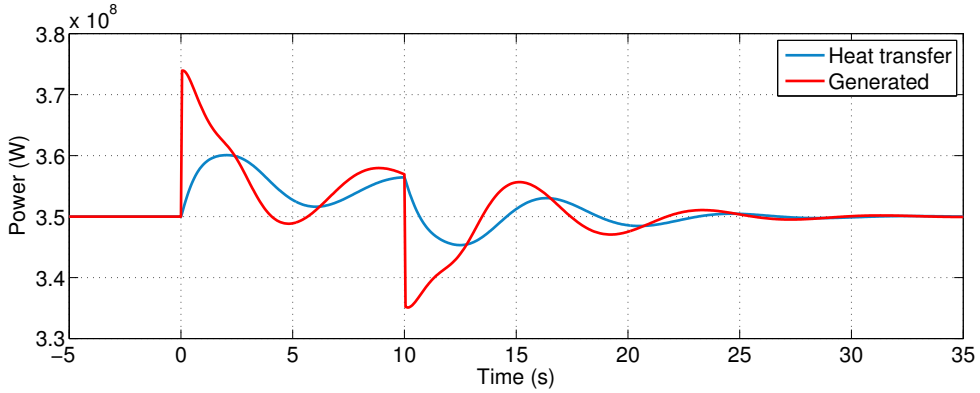

Figure C.2: Response of the power generated and heat transfer to the coolant as a response to a reactivity insertion of 100 pcm for 10 seconds with $D_{\text{pin}} = 32mm$.